Simulation of crystallization of isotactic polypropylene with different shear regimes

Simulation of crystallization of isotactic polypropylene with different shear regimes

Roberto Spina [1,2#], Marcel Spekowius [2,3] and Christian Hopmann [2]

[1] Dept. of Mechanics, Mathematics and Management (DMMM), Politecnico di Bari, Viale Japigia 182, 70126, Bari, Italy.

[2] Institute of Plastics Processing (IKV), RWTH Aachen University, Pontstraße 55, 52062, Aachen, Germany.

[3] Contien GmbH, Merzbrück 214, 52146 Würselen, Germany

[#] Corresponding Author / E-mail: roberto.spina@poliba.it, Tel/fax: +39 080 5962768.

Abstract

Flow induced crystallization is an important process during polymer solidification because it strongly influences the material morphology and properties. The melt of isotactic polypropylene crystallizes slowly in isothermal conditions whereas shear conditions speed up the crystallization process. The main objective of the presented research is the investigation of the shear-induced crystallization of isotactic polypropylene through a comparative analysis between isothermal and non-isothermal conditions in different shear regimes. A numerical simulation of crystallization kinetics of semicrystalline thermoplastics with a multiscale model is proposed to evaluate the nucleation and growth of spherulites, after identifying the material parameters needed to connect crystallization kinetics to the molecular material properties. This model is validated by using data from differential scanning calorimetry (DSC) and a rotational rheometry (RHEO).

Keywords: Polymer, Crystallization, Multiscale.

1. Introduction

The uses of polypropylene (PP) are numerous because of how versatile this material is. According to the data report of the *Association of Plastics Manufacturers* [**1**], PP is one of the most important polymers with revenues expected to exceed €130 billion by 2019. The demand for this material grew at a rate of 4.8% per year between 2004 and 2015. The European market for this material in 2016 was about 9.1 million tons out of a total demand for plastics of 49 million tons. Packaging, building/construction and the automotive sector are the top three markets. In terms of number of applications, 2576 have been recorded in the automotive sector, 1033 in household goods, 757 in containers, 712 in appliances, 673 in film, 671 in electrical/electronic applications, 658 in packaging, 627 in automotive interior parts and 573 in general purpose, according to statistics of *UL Prospector* [**2**]. PP has demonstrated certain advantages in improved strength,

stiffness and higher temperature capability over other commodity polymers, allowing its use in everyday applications.

For this reason, the crystallization of PP is a very important issue for all the technological processes involving the melting, shaping and cooling of this material. The final product properties strictly depend on the influence of the complex thermo-mechanical history on microstructure development. PP is a polymorphic polymer that can have several crystal modifications depending on processing conditions (temperature, pressure, time, etc.) as well as isotacticity. Unlike polyethylene, which crystallizes in the planar zigzag form, the presence of the methyl groups on the chain promotes the crystallization of the isotactic PP in a helical form, as *Harper* reports [**3**]. Commercial PPs are approximately 90 to 95% isotactic. The amount of isotacticity present in the chain influences the final properties. An increase of the isotactic fraction causes an increase in crystallinity, thus raising the material modulus, softening point and hardness.

If we focus our attention on injection molding and extrusion, which represent most of the leading manufacturing processes of PP, the thermo-mechanical history mainly consists of flowing molten material into a mold/die to give the desired shape and then cooling it to the room temperature to achieve the final dimensional stability. Concerning the melt viscosity, it is very dependent on the shear rate. An increase in the velocity decreases the processing time but increases the shear rate, which can lower the viscosity of the polymer during processing and thereby provide a better chain entanglement and promote crystallization. As for the cooling rate, the main effect is that crystallization is very fast for temperatures between the melting point and the glass-transition. As the temperature is reduced below the glass transition, the crystallization rate rapidly decreases because of the reduction in molecular movement. Crystallization takes place during the cooling phase for 60-80% of the total amount whereas the remaining fraction crystalizes after processing. Crystallization can take anything between a very short time and up to several weeks to be completed, depending on environmental conditions, until a stable crystal structure is achieved. Since polymer crystallization is significantly influenced by the above processing conditions, the measurement of a characteristic crystallization temperature should be carried out under the same conditions realized during polymer processing. Because these conditions are not easy to apply, the simulation of the process with crystallization behavior is highly desirable. Even if this behavior is relatively well-documented, there are very few 3D process-independent multiscale models.

In this work, the influence of the processing history on the morphology and final properties of isotactic PP have been studied by combining an experimental and numerical approach. The material was shaped into disks with no-flow and high cooling rates and then isothermal and non-isothermal conditions were applied, coupled to different shear regimes. We focus on the effect of the resulting thermo-mechanical history on the structuring of the material and, in particular, on the role of shear

regime on micro-structural development. This work was carried-out by studying the same behavior with two different instruments, DSC and RHEO, reproducing phenomena with a multiscale simulation model that can be easily extended to the injection molding and extrusion processes.

2. Research background

The current research on polymer crystallization is focused in how flow influences industrial conditions. Crystallization of polymers, which involves two consecutive phenomena (nucleation and growth), is governed by both thermodynamic and kinetic considerations. Broadly speaking, polymer crystallization under processing conditions cannot be considered an equilibrium phenomenon, since it is not possible to separate the thermodynamic effects on the processes from the kinetic ones, as *Brucato and La Carruba* mention [**4**]. The approaches used to investigate crystallization can be classified into experimental and numerical.

Following the experimental path, observations with a polarized microscope coupled to a rheometer or a thermal shearing device are the most used investigation techniques. *Vega et al.* [**5**] evaluated the effect of shear flow on crystallization in combination with molecular architecture and determined the different regimes as a function of the flow history. Their work started from the observation that flow gradients strongly affected the crystallization process, and, viceversa, the latter affected the rheological behavior. For this reason, rheometry can be a complementary tool to couple with differential scanning calorimetry in studying the microstructure evolution during crystallization. *Koscher and Fulchiron* [**6**] investigated the shear effect on the crystallization with a polarized light microscopy and a shearing hot stage. A model was developed to predict the crystallization kinetics, considering that the sensitivity of crystallization kinetics to the shear depended on polymer rheology, in general, and on molecular weight distribution, in particular. Qualitative predictions of the crystallization behavior of polypropylenes with different molecular weight distributions to the shear treatment were carried-out. *Coccorullo et al.* [**7**] measured the nucleation and growth rates of spherulites during continuous and constant steady shear flow with a thermal shearing cell coupled with an optical microscope. They investigated the effect of a steady shear flow on the morphology evolution and the kinetics of isothermal crystallization. The main result was that the nucleation density in no-flow conditions remained constant with time. No nucleation rate was observed during the test while an increase in nucleation density with time was observed under shear flow. *Chen et al.* [**8**] presented a study in which a rotational rheometer was used to characterize the shear effect on the rate of polymer crystallization. Steady-shearing experiments revealed that the upturns of shear stress and normal force could be used to quantify the rate of crystallization. Special attention was paid to temperature-invariant scaling parameters to determine the shear effect on the rate of isothermal crystallization. *Pantani et al.* [**9**] carried-out

experiments of nucleation density and the growth rate of spherulites under continuous shear in specific ranges of temperature and shear rate. The effect of flow on nucleation and growth rates was attributed to the increase in the melting temperature. For this reason, the growth rate Hoffman-Lauritzen equation was valid under flow conditions by including the effect of shear rate on the melting temperature. *Hamad et al.* [**10**,**11**] investigated the crystallization kinetics of several linear isotactic polypropylenes by varying shear and quench temperatures as well as shear rate and duration, and monitoring crystallization after quenching. New experiments on both the crystallization kinetics and crystal morphology (which, in addition to spherulites, also involved rice grains) were reported. The main result was the identification of the saturation magnitude of flow-induced speed up correlated with the tacticity. Moreover, experimental observations suggested that both stretched chains and particulate impurities had a great influence on flow-induced crystallization. *Ziabicki and Sajkiewicz* [**12**] proposed a crystallization model taking into account the relaxation time and the athermal nucleation function. The research results report an important acceleration of crystallization due to fast cooling conditions, identifying athermal nucleation as the main factor causing this acceleration. *Toda* [**13**] proposed a method based on periodically modulated driving force in which supercooling was modulated in a periodic manner and the kinetic response was analyzed. The mai result of this research was computation of the temperature dependence of growth rate, useful to determine the surface free energy for the nucleation process.

Following the numerical path, several approaches were developed and implemented. *Zinet et al.* [**14**] used the experimental data presented by *Koscher and Fulchiron* [**6**] to develop a numerical model able to simulate the crystallization of polymers under non-isothermal flows. The authors observed that the sensitivity of the crystallization kinetics to the flow was a consequence of the flow dynamics and the rheological behavior of the melt. The model also gave information about the final crystalline structure in terms of relative distribution of thermally and flow induced crystallites and their mean sizes. *Durin et al.* [**15**] proposed a general numerical method to simulate polymer crystallization under various conditions. The methodology combined a theoretical approach and numerical simulation based on the general framework of overall kinetic theories, initially developed for metals. The application was applied to polymers by imposing the growth rate as a function of temperature, with spherulite growth governed by an interfacial mechanism and not diffusion-controlled. *Guo and Nahr* [**16**] proposed a stress-induced crystallization model for semicrystalline plastics in which an increase in the melting temperature of thermoplastics was caused by stress-induced orientation of molecules and chains. Therefore, the super-cooling was the driving force for crystallization and the equilibrium melting temperature shifted to higher temperatures in the stressed or oriented state. *Jarecki and Misztal-Faraj* [**17**] developed a kinetic model in which lamellar thickness distribution and average lamellar thickness during melt crystallization were

evaluated. The model involved thermal thickening which accounted for lamellar doubling transformation and logarithmic thickening of the doubled crystals. The model could compute the time development of the lamellar thickness distribution during melt isothermal crystallization. *Liu et al.* [**18**] proposed the reduction of the computation complexity in studying crystal interaction by using the level set method. The authors presented a new approach in which the level set method was used by solving a single signed distance function with the aid of colors as crystal identifiers. Each crystal was identified by its assigned color. The advantages of this approach were its easy implementation, low computational complexity and low memory requirement. *Raabe and Godara* [**19**] developed a three-dimensional model with a probabilistic cellular automaton to predict the kinetics and topology of spherulite growth during crystallization. A switching probability of the cells was formulated according to the kinetic theory of Hoffman and Lauritzen after tuning it with experimental data coming from previous research. The model correctly computed the kinetics of instantaneous homogenous nucleation under isothermal no-flow conditions and under weak shears. *Spina et al.* [**20**,**21**] implemented a robust framework for the computation of the crystallization kinetics of semi-crystalline thermoplastics in injection molding by using a multiscale approach. The purpose was to assess parameters influencing microstructure formation that would otherwise require very time-consuming analysis with experiments. The numerical method, crystallization kinetics and their implementation into numerical software operating at macro- and meso-scale were described as well as the experimental data needed to prepare and validate numerical results.

3. Materials and Methods

Physical phenomena can be modeled at varying degrees of complexity and at different scales. Multiscale modeling provides a framework, based on fundamental principles, for constructing mathematical and computational models of crystallization, by examining the connections between models at different scales, as stated in *Weiman* [**22**]. To achieve successful results, reliable material data was necessary, especially when it is necessary for the material properties to be controlled in every step of the process (*Heaney and Spina* [**23**]). The analysis of the material was carried-out by initially defining the main protocol of investigation and then a common reference. In this way, data becoming from different devices could be easily matched and compared with numerical results.

3.1 Experimental activity

Experimental data were collected at different levels to achieve reliable simulation computations. Crystallization of PP was investigated in several scenarios, considering flow/no-flow and isothermal/non-isothermal conditions. The two methods of analysis employed were DSC and

RHEO. The flow diagram of the experiment protocol is reported in Figure 1 and the imposed thermal cycle is represented in Figure 2.

- - - Figure 1: Experiment flow diagram - - -

- - - Figure 2: Thermal Cycle - - -

In DSC experiments, the material (3.0±0.1 mg) was placed into a standard aluminum pan (99.5% Al, maximum dimension of ∅ 6.7 mm with a volume of 85 µl). A DSC Q2000 (TA Instruments, New Castle, USA) was employed, using liquid nitrogen as cooling media. The sample was heated from room temperature $T_{ambient}$ to temperature T_{up} greater than melt temperature T_{melt} with a constant heating rate dT/dt_{heat}, kept at this temperature for a sufficient time t_{up} (5.0±0.1 min) to destroy any crystalline microstructure prior to the experiment and then cooled to the plateau temperature $T_{plateau}$ (isothermal case) or $T_{ambient}$ (non-isothermal case) with a constant cooling rate dT/dt_{cool}. In the isothermal experiment, $T_{plateau}$ was kept constant for holding time $t_{plateau}$ sufficient to achieve the full crystallization, and then cooled to $T_{ambient}$ with the same cooling rate as the previous step. $T_{plateau}$ was in the range 120-140 °C and $t_{plateau}$ was in the range 30-120 min. Attention was paid to temperature undershot to prevent a premature start of crystallization. In fact, two main requirements were fulfilled: i) the sample was cooled very quickly to prevent crystallization from starting during cooling and ii) the temperature was stabilized at $T_{plateau}$ without any under- or overshooting. The cooling rate values were not comparable with those of a fast differential scanning calorimetry (*Schawe et al.* [**24**], *Mileva et al.* [**25**]). Three repetitions were carried-out to reduce the sensitivity of crystallization tests due to polymer properties.

The RHEO measurements were made with the same thermal cycle described above. All experiments were performed on a HAAKE MARS III rotational rheometer (Thermo Fisher Scientific Inc, Waltham, USA), using nitrogen as shielding gas to avoid polymer degradation and water as cooling media. The material (initially in the form of pellets) was placed between the two highly polished stainless steel plates of the shearing device at $T_{ambient}$, heated to T_{up} and held for t_{up} for a complete melt. The distance between the two plates was reduced to 0.1 mm by slowly lowering the upper measuring geometry to produce a disk with a diameter of 25.0 mm. This gap was kept constant during all the subsequent steps of the thermal cycle, compensating for variations caused by thermal expansion by automatically moving the upper measuring geometry in the axial direction. In this way, the contact between the polymer and the upper plate was always guaranteed. In a no-flow condition, the experiment was similar to the DSC one, selecting the isothermal or non-isothermal case. When flow was required in the non-isothermal case, shear $dγ/dt$ was immediately applied after t_{up} with a step function with a duration equal to t_{shear}. On the contrary, the delay t_{start}

was applied in the isothermal case and the step function started once the T_{up} had been reached. Temperature sweeps were carried-out with $d\gamma/dt$ equal to 0.0-1.0 rad s^{-1}. Precise control of the under- or overshooting conditions during the switch between cooling and isothermal step was performed, considering the difference between the masses of the sample disk and shearing plates and the interaction with the cooling media (distilled water).

3.2 Multiphysics modeling

The numerical analysis made use of a finite element (FE) model at macro-level designed using COMSOL Multiphysics (Comsol Inc., Burlington, USA). Computational flow dynamics, heat transfer and structural mechanics were the main physics used in the FE model, the geometrical domain of which was a disk with radius R_d and height Z_d in cylindrical polar coordinates (r, φ, z). The governing equations were the continuity, momentum and energy in a non-isothermal incompressible flow simulation problem:

	$\nabla \cdot \underline{u} = 0$	(1)
	$\rho\left(\frac{\partial \underline{u}}{\partial t} + \underline{u} \cdot \nabla \underline{u}\right) = -\nabla p + \nabla \cdot \underline{\underline{\tau}} + \rho \underline{g}$	(2)
	$\rho c_p \left(\frac{\partial T}{\partial t} + \underline{u} \cdot \nabla T\right) = \nabla \cdot (k \nabla T) + \underline{\underline{\tau}} : \nabla \underline{u} + U_{cryst}$	(3)

where $\underline{u}$ is the velocity vector, p the pressure, $\underline{\underline{\tau}}$ the stress tensor, ρ the density, $\underline{g}$ the gravity vector, c_p the specific heat, k is the heat conduction and U_{cryst} the heat of crystallization. The stress tensor was related to the viscosity η through the Stokes stress constitutive equation

	$\underline{\underline{\tau}} = \eta \cdot [\left(\nabla \underline{u}\right) + \left(\nabla \underline{u}\right)^T]$	(4)

The crystallization process at macro-scale level was initially modeled using the non-isothermal Johnson-Mehl-Avrami-Kolmogorov (JMAK) equation

	$\xi = 1 - exp[-K(T)t]^n$	(5)

coupled to the Nakamura crystallization rate

	$\frac{\mathrm{d}\xi}{\mathrm{d}t} = nK(T)(1-\xi)[-ln(1-\xi)]^{\frac{n-1}{n}}$	(6)

where the degree of crystallization ξ was a function of the Avrami exponent n and the overall non-isothermal kinetic rate constant $K(T)$. The exponent n was

	$n = m + g$	(7)

where m was associated to nucleation (0 for instantaneous and 1 for random/sporadic) and g to the dimension of growth (3 for spatial, 2 for planar and 1 for linear growth). The term $K(T)$ was a function of the half time $t_{½}$

	$K(T) = \frac{ln(2)^{\frac{1}{n}}}{t_{1/2}}$	(8)
	$\frac{1}{t_{1/2}} = \frac{1}{t_{1/2,0}} exp\left[-\frac{U^*}{R\left(T\text{-}T_g + T_\infty\right)}\right] exp\left[-\frac{\kappa_t \left(T_{m,0}\right)^2 \left(T_{m,0} + T\right)}{2T^2 \left(T_{m,0}\text{-}T\right)}\right]$	(9)

where $t_{½,0}$ was the half time in equilibrium condition, U^* the activation energy for the segmental jump rate in polymers, R the ideal gas constant, κ_t the parameter associated to the spherulite growth rate, $T_{m,0}$ the equilibrium melt temperature, T_g the glass transition temperature and T_∞ the temperature below which the diffusion stops. The half time $t_{½,0}$ was a pre-exponential factor including all terms independent of temperature. The above equations were valid for material in melt condition. In partial solid state, the deformation of the samples in the investigated experiments resembled the torsion of a disk. The material properties were dependent on the material state (*melt*, *solid*), process variables (pressure and temperature) and degree of crystallization. The boundary conditions were the velocity and temperature fields imposed by the system. In particular, no inlet and outlet existed because the material could not enter or exit from the system. Non-slip conditions were imposed on the two plate geometries, whereas the fluid to air boundary condition was specified as slip. The upper plate was defined as a moving wall with tangential velocity $\omega \times r$ whereas the lower plate was fixed. Two proportional-integral-derivative (PID) controllers were used in simulations to reproduce the temperature variation and the velocity impulse of the experimental tests. The temperature was varied by using two volume heat sources, one for each plate, and evaluating the PID with

	$Q(t) = K_{pro,T}\Delta T(t) + K_{int,T}\int_0^t \Delta T(t)dt + K_{der,T}\frac{\mathrm{d}\Delta T(t)}{\mathrm{d}t}$	(10)
	$\omega(t) = K_{pro,\omega}\Delta\omega(t) + K_{int,\omega}\int_0^t \Delta\omega(t)dt + K_{der,\omega}\frac{\mathrm{d}\Delta\omega(t)}{\mathrm{d}t}$	(11)

where $\Delta T(t)$ is the difference between the set and real temperature, $\Delta\omega(t)$ the difference between the set and real angular velocity, the coefficients $K_{pro,T\ th}$ $K_{int,T}$ and $K_{der,T}$ the controller tuning parameters for the temperature and $K_{pro,\omega}$, $K_{int,\omega}$ and $K_{der,,\omega}$ *the* controller tuning parameters for the angular velocity.

The meso-model was implemented using an in-house software SphäroSim (IKV, Aachen, Germany). The software employed Cellular Automata (CA) to compute the nucleation and growth of the spherulites in a cell, based on temperature and velocity fields estimated from the FE model. The input data, in terms of scalar and vector fields calculated with the FE model, was transferred and computed at the nodes of the mesh. Each hexahedron element of the FE mesh was subdivided into a high-resolution mesh of cubic cells with an edge length λ, normally 100 times smaller than the edge length of the FE mesh. A cell could take two discrete state values such as *melt* or *solid* and an event-based approach was used to switch between these two states. An event represented a point in time at which a state change of at least one cell happened with a sufficiently high probability. In a nucleation event, nuclei were statistically distributed over the cells of CA whereby the calculation of the probability distribution was carried-out. Whenever the state of a cell changed from *melt* to *solid*, growth events were created for the neighborhood of this cell. The growth events were used to calculate the state changes because of the crystal growth process. Nucleation and growth events were successively executed to simulate the complete solidification process. The basic equation of the nucleation rate v_n and growth rate v_g were

$$v_n = Ck_bT\Delta G exp\left(-\frac{E_a}{RT}\right) exp\left(-\frac{K_{nuc}}{T\Delta G^{n_{nuc}}}\right) \quad (12)$$

$$v_g = v_{g,0} exp\left[-\frac{U^*}{R\left(T-T_g+T_\infty\right)}\right] exp\left[-\frac{\kappa_g\left(T_{m,0}\right)^2\left(T_{m,0}+T\right)}{2T^2\left(T_{m,0}-T\right)}\right] \quad (13)$$

with C and K_{nuc} material constants, k_b the Boltzmann constant, ΔG the free Energy, E_a the energy barrier of the nucleation, $v_{g,0}$ a material constant, κ_g the parameter associated to the spherulite growth rate and n_{nuc} the geometrical factor for the nucleation model. The Gibbs free energy ΔG was split into a no-flow part ΔG_q and a flow-induced part ΔG_f, which can be calculated from the given temperature and velocity fields, as below reported

$$\Delta G_q = H_0\left(1-\frac{T}{T_{m,0}}\right) \quad (14)$$

$$\Delta G_f = \frac{3}{4}\frac{Ck_bT}{\pi}\int_{-\infty}^{t}\dot{\mu}(t,t_i)dt_i\int ln\left(\left|E(t,t_i)\cdot \underline{I}\right| d\underline{I}\right) \quad (15)$$

where H_0 is the latent heat of crystallization, where $\mu(t,t_i)$ is the Doi-Edwards memory function, $E(t,t_i)$ the deformation tensor between the times t_i and t and I a unit pseudo-vector associated to a primitive chain segment. ΔG_q was derived from steady-state conditions whereas the reptation theory of *Doi ed Edwards* [**26**] was applied for the flow induced part ΔG_f (*Spekowius et al.* [**27**]).

The crystallization degree was computed by comparing the number of cells N_{Solid} in solid states with the total number of cells N_{Total} in the simulation area.

$$\xi = \frac{N_{Solid}}{N_{Total}} \quad (16)$$

4. Model preparation

The simulation of the flow and solidification process required the identification of the material-specific properties. For this reason, the first part was dedicated to calibrating the material model with the experimental data. The second part was devoted to designing and setting the numerical models at macro and meso levels

4.1 Calibration of the material model

The PP 505 P produced by SABIC AG (Bergen op Zoom, Netherlands) was used as the semi-crystalline thermoplastic polymer for the present investigation. This material is an isotactic polypropylene with a specific density of 0.905 g/cm^3 at room temperature and melt flow index of 2.0 g/10 min. The DSC data was used to calibrate the macro- and meso-model in isothermal and non-isothermal conditions.

One of the main important variables to be identified was the equilibrium half time $t_{½}$. Assuming that crystallization did not take place during cooling in the isothermal case, the variable was extrapolated from the isothermal DSC curves with T_{up} equal to 180 °C, constant cooling rate dT/dt_{cool} of 20 °C/min, $T_{plateau}$ ranging from 135 to 120 °C and $t_{plateau}$ of 120 min. The half time was computed using

$$\frac{1}{t_{1/2}} = \frac{1}{t_{1/2,0}} exp\left[-\frac{U^*}{R\left(T-T_g+T_\infty\right)}\right] exp\left[-\frac{\kappa_t\left(T_{m,0}\right)^2\left(T_{m,0}+T\right)}{2T^2\left(T_{m,0}-T\right)}\right] = \sqrt[4]{\frac{\pi v_n {v_g}^3}{3ln(2)}} \quad (17)$$

where the left- and right-hand sides of the equation was related to the macro and meso models respectively. The resulting curves are reported in Figure 3 and the half-time as a function of the plateau temperature $T_{plateau}$ is reported in Figure 4, together with the experimental data of *Lamberti* [**28**].

- - - Figure 3: Isothermal DSC curves - - -

- - - Figure 4: Isothermal half-time - - -

The half-crystallization times were also computed for non-isothermal cases. The measured DSC curves are shown in Figure 5 whereas the crystallization half-time as a function of the cooling rate is represented in Figure 6.

- - - Figure 5: Non-isothermal DSC curves - - -

- - - Figure 6: Non-isothermal half-time - - -

The equilibrium half time $t_{½}$ was also identified for the RHEO experiments, after calibrating the device using Indium for the temperature reference. The variation of the storage modulus was used to computed the crystallization degree by using the following equation proposed by *Khanna* [**29**]:

$$\xi = \frac{G'(T) - G'(T_{m,0})}{G'(T_{ambient}) - G'(T_{m,0})} \quad (18)$$

where $G'(T_{m,0})$, $G'(T)$ and $G'(T_{ambient})$ were the melt stiffness values at *0*, *t* and infinity time. The crystallization curves produced in the RHEO experiments were very close to the DSC ones. The $G'(T_{ambient})$ was compute using the following equation proposed by *Eckestein et al.* [**30**] with:

$$G'(T_{ambient}) = \frac{\rho RT}{M_e} \quad (19)$$

where ρ is the polymer density and Me the molecular entanglement molecular weight.

The second main parameter to identify was the growth speed at equilibrium $v_{g,0}$. The calibration of the growth model was carried out by using several images of a polymer melt crystallizing in isothermal conditions, captured with a polarized light microscopy mounted on the RHEO device. The same experimental protocol adopted for the DSC analysis was used and the growth of individual spherulites over time was observed. The growth speed was determined by evaluating changes in the spherulite diameters. The main assumptions of this method were that the crystallization did not take place during cooling and the growth of individual spherulites could be observed at the plateau temperature. Moreover, the idea of *Lamberti* [**31**] of describing the isothermal growth speed of various isotactic polypropylenes through a master curve was adopted. The material parameters of Table 1 was thus used to compute the master curve. Figure 7 shows some snapshot at different times of the polymer melt in no-flow conditions and relative measurements of the observed spherulites. Figure 8 reports the evolution of the storage modulus *G'*, loss modulus *G''* and phase angle δ during the same experiment.

- - - Figure 7: Polymer melt during cooling- - -

- - - Figure 8: Rheometer curves - - -

The success of the material model in predicting experimental data by using results obtained from *Ratajski and Janeschitz-Kriegl* [**32**] was confirmed, as Figure 9 shows. It is possible to note that a good agreement for both isothermal and non-isothermal conditions exists between the experimental data and the material model, the parameter values of which are reported in Table 1. The material data was coherent with that computed in previous researches by *Lamberti* [**31**], *De Santis et al.* [**33**] and *Qiu et al.* [**34**].

- - - Figure 9: Growth speed - - -

- - - Table 1: Parameters of the material model - - -

4.2 Design of the numerical models

The geometrical domain of the macro FE model was a disk with a radius R_d of 12.5 mm and height Z_d of 0.1 mm, with a volume of about 49 mm^3. The numerical simulations were performed using a three-dimensional model. Some preliminary runs were carried-out to select the average distribution of elements along the radius and the thickness for a correct balance between simulation speed and accuracy. As a result of these initial simulation runs, an optimal distribution of the FE mesh was identified and it consisted of 5 elements across the thickness and a maximum mesh length of 1.0 mm along both radius and circumference, for a total number of quadratic elements equal to 4,000 (3,600 hexahedra and 400 prisms). The FE mesh used in the following computations is shown in Figure 10.

- - - Figure 10: FE Mesh - - -

To complete the model, boundary conditions were specified at all model surfaces. The main boundary conditions were: i) the velocity normal to the upper and lower surfaces was zero; ii) the upper surface rotated with an angular velocity $\omega(t)$ around the vertical axis, perfectly transmitted by the upper plate with no-slip condition; iii) the velocity at the lower surface was different from zero along the parallel direction, according to a specific slip value of polymer/steel interface; iv) the temperature profile was imposed by varying $Q(t)$ and v) the side surface was unconstrained. Figure 11 reports the displacement results in no-flow (left side) and under flow (right side) conditions with a plateau temperature $t_{plateau}$ of 125 °C and a shear rate of 7.854 1/s at 6.25 mm from the disk center. The flow lines in a no-flow condition were oriented towards the center of the disk because of thermal contraction. The flow lines were oriented in concordance with the imposed rotation vector.

- - - Figure 11: Displacement - - -

The Volume of Analysis (VOA) in the middle of the macro model was used to to evaluate the effects of crystallization and compute the shear condition (Figure 12). The geometry of the meso-model was a cube with an edge length of 100 μm and a volume of 10^6 μm^3.

- - - Figure 12: Volumes of analysis - - -

In this case, the maximum mesh length of the meso-model was equal to 1.0 μm, for a total number per hexahedra equal to 10^6 cubic cells. The choice of this high number of cubic cells was justified by the need to identify the variations of the flow front and temperature gradients with a high level of details. The two boundary conditions of the meso-model used for the confined spherulite growth with CA were the fixed or periodic condition. In the formal definition of CA, it is reasonable and necessary to consider the lattice as infinite in all dimensions. However, a truly infinite lattice was impossible to simulate and boundary conditions were needed. Fixed conditions were obtained by imposing a specific value on the boundary cells. This value, determined from the application, confined the spherulite growth along the wall. Periodic boundaries were prescribe by extending the lattice through the addition of cells to the original structure and mirroring them, copying one row/column to the opposite edge. No cell in this topology could reach the boundary in any way and thus it was closest to an infinite lattice. The mirroring was possible as part of the hypothesis that the velocity and temperature did not change much in the mirroring direction. The procedure is shown in Figure 13 for a 2D representation. The area of observation consisted of a 8×8 cells in which three spherulites were present at time t_i. In the following time step, the cells were added to correctly computed the spherulite growth and mirrored along the periodic boundary with respect to the vertical axis located at the middle of the area of observation. The procedure was repeated until the entire area was covered by the spherulites. The same figure shows one of the advantages of this meso-scale simulation, namely the accurate detection of the point in time of a contact between the different growth fronts of spherulites, enabling the identification of interface layers for further analysis.

- - - Figure 13: Spherulite growth - - -

One important aspect to underline is that the evolution of the spherulite considered the nucleation and growth events. As far as nucleation is concerned, a probability distribution was calculated taking into account the local nucleation rates. This computation required the determination of the

Gibbs free energy in each cell of the cellular automaton, taking into account the no-flow and flow conditions. The crystal growth speed was only dependent on material parameters and the local temperature. An integration along the growth path over the time was performed to convert the speed into one of the possible states of the cellular automaton, describing the direct connection from the nucleus of the spherulite to the current growth front.

5. Analysis of results and discussions

The crystallization kinetics in no-flow conditions were initially analyzed by comparing computations of the macro and meso-models with the DSC experiments. The results of the macro-model are shown in Figure 14 in terms of the crystallization degree ξ as a function of the time for a no-flow isothermal case ($T_{plateau}$ equal to 130°C). The crystallization degree was homogeneous in all specimen points due the reduced thickness.

- - - Figure 14: Crystallization degree at 130°C \ Macro-model - - -

A 3D representation of the growth of spherulites is given in Figure 15. In this figure, the evolution of the crystallization degree (space filing) of the investigated VOA as a function of time for $T_{plateau}$ equal to 130°C is shown.

- - - Figure 15: Crystallization degree at 130°C \ Meso-model - - -

A good agreement was achieved between JMAK, Sphaerosim and DSC data with very few differences in terms of curve shapes. This behavior can be explained by considering that the macro and micro models were accurately calibrated with the experimental data. The JMAK model adequately describes the bulk crystallization kinetics but its phenomenological modeling does not allow the molecular-level description of the processes taking place during crystallization. On the contrary, the meso-model allows the spherulite size and distribution to be computed. A comparison of the evolution of the spherulites computed for the VOA for $T_{plateau}$ equal to 125, 128 and 130°C is shown in Figure 16.

- - - Figure 16: Spherulite evolution \ isothermal - - -

In the examined range, at lower temperature, the crystallization process was characterized by a high nucleation rate and rapid growth of the spherulite dimensions. On the contrary, at higher temperatures the nucleation rate was low as well as the growth rate. A greater undercooling lowered

the activation energy for nucleation, causing a higher concentration of nuclei and a faster crystallization. As a result, the number of spherulites at the end of process at 125, 128 and 130°C were respectively 102, 73 and 45 respectively, confirming that the spherulite density increased with time and decreased with $T_{plateau}$. As for the mean spherulite dimensions, the results highlights that when crystallization started, the spherulite dimensions were low and distribution was narrow. During growth, the distribution became wider. Figure 17 shows the distribution of the spherulite size at the end of the process. The mean spherulite size was approximately 50 µm, in accordance with measurements reported in Figure 7.

- - - Figure 17: Spherulite size distribution \ isothermal - - -

The computation was then performed with a $T_{plateau}$ equal to $T_{ambient}$. In this case, a non-isothermal test was investigated with crystallization started during the cooling ramp. The total number of spherulites identified at the end of crystallization was 6, very fews compared to the above isothermal cases. The nucleation rate was also very low whereas the growth speed was high. As a result, the spherulites nucleated in the first step of the process grew very quickly, reaching a large size, whereas the following nuclei did not have enough space to reach considerable dimensions. Figure 18 shows this simulation scenario.

- - - Figure 18: Spherulite evolution \ non-isothermal - - -

The crystallization kinetics were then investigated in isothermal conditions with variable shear regimes. Higher temperatures caused lower relaxation times and consequently lower orientations, as reported by *Coppola et al.* [**35**]. This fact, together with the intrinsic temperature effects on no-flow crystallization kinetics, could cause a significant coupling between temperature and flow even under isothermal conditions, when temperature does not change with time. The polymer chains oriented faster, and when the flow is stopped, they recoil faster as well, as *Gooneie et al.* [**36**] report. The investigated scenarios considered the same $T_{plateau}$ temperature with shear rates ranging from 0 to 10 1/s, computed at the middle of the disk. Figure 19 reports the evolution of the crystallization degree (space filing) of the simulations results as a function of time for $T_{plateau}$ equal to 125°C and shear regimes equal to 0, 1 and 10 1/s.

- - - Figure 19: Crystallization degree at 125°C - - -

The experimental DSC curve at $T_{plateau}$ is reported in the same figure, confirming the excellent agreement between the experiments and meso-model computations for zero shear rate. A good agreement was also attained with the experimental RHEO curve for a shear rate equal to 10 1/s, confirming the good predictions of the macro- and meso-models. The results, achieved with shear rates equal to zero and 10 1/s respectively, confirmed that shear deformations increased the nucleation density and the crystallization kinetics, respectively, leading to the completion of the crystallization in a shorter time. This outcome is more evident in Figure 20, reporting the spherulite evolution over time by using the same time steps.

- - - Figure 20: Spherulite evolution at 125°C \ Shear influence - - -

It is possible to note that at the initial step of analysis (225s), the number of spherulites was 39 and 44 respectively for zero and 10 1/s.

The nucleation rate was higher with a higher shear rate. Thus, there were more spherulites growing which increased the space filling rate. The results highlight that flow induced the local orientations of polymer chains, thus enhancing the nucleation rate. For this reason, temperature played an important role in affecting the polymer relaxation times. The same behavior was identified for non-isothermal case. Figure 21 shows the results achieved whit in no-flow conditions and with a shear rate equal to 10 1/s.

- - - Figure 21: Spherulite evolution at 25°C \ Shear influence - - -

The flow promoted the nucleation and growth of the crystallization process, which started and was completed faster than that recored in no-flow conditions. In addition, the final number of spherulites was 12 and 43, respectively for shear rates equal to 0 and 10 1/s. The higher the number of spherulites was, the lower was the spherulite radius.

6. Conclusions

The paper reports the development a computationally-accessible macro\micro-model for flow-induced crystallization in thermoplastic polymers. A micro-model based on cellula automata was implemented and then linked to the macro-model level used to represent the process. A detailed description of the crystallization kinetics was produced based on the microscopic free energy definition and material properties. The performance of the proposed macro-micro model was calibrated using the DSC and RHEO experimental data in various no-flow/non-isothermal and flow/no-flow conditions. The calibrated model was able to compute crystallization at coarse and

fine scale, reproducing with a good agreement for all process conditions. Additional experimental work should improved the model predictions by considering athermal contribution to crystallization.

Acknowledgment

It is a pleasure to thank Prof. Luigi Tricarico (DMMM - Politecnico di Bari) for his precious support during the research activities.

The authors acknowledge funding for this work from the Deutsche Forschungsgemeinschaft (DFG) as part of the program Cluster of Excellence "*Integrative Production Technology for High-wage Countries*" at RWTH Aachen University and the Italian National Operative Program as part of the SMATI project (PON01_02584).

References

[1] Plastics - the Facts 2016, http://www.plasticseurope.org/information-centre/publications.aspx, 2017 (accessed 01.03.2017).

[2] Polypropylene. http://plastics.ulprospector.com/generics/39/polypropylene-pp, 2017 (accessed 01.03.17).

[3] C.A. Harper, Modern Plastics Handbook, McGraw-Hill, New York, 1999.

[4] V. Brucato, V. La Carruba, Solidification of Polypropylene Under Processing Conditions - Relevance of Cooling Rate, Pressure and Molecular Parameters, in: Polypropylene, InTech, Vienna, 2012, 429-458.

[5] J.F. Vega, D. Hristova, G.W.M. Peters, Flow-induced crystallization regimes and rheology of isotactic polypropylene. J. of J. Therm. Anal. Calorim. 98 (2009) 655-666.

[6] E. Koscher, R. Fulchiron, Influence of shear on polypropylene crystallization: morphology development and kinetics, Polym. 43 (2002) 6931-6942.

[7] I. Coccorullo, R. Pantani, G. Titomanlio, Spherulitic nucleation and growth rates in an iPP under continuous shear flow, Macromolecules 41 (2008) 9214-9223.

[8] Q. Chen, Y. Fan, Q. Zheng, Rheological scaling and modeling of shear-enhanced crystallization rate of polypropylene, Rheol. Acta 46 (2006) 305-316.

[9] R. Pantani, I. Coccorullo, V. Volpe, G. Titomanlio, Shear-induced nucleation and growth in isotactic polypropylene, Macromolecules 43 (2010) 9030-9038.

[10] F.G. Hamad, R.H. Colby, S.T. Milner, Onset of flow-induced crystallization kinetics of highly isotactic polypropylene, Macromolecules 48 (2015) 3725-3738.

[11] F.G. Hamad, R.H. Colby, S.T. Milner, Transition in crystal morphology for flow-induced crystallization of isotactic polypropylene, Macromolecules 49 (2016) 5561-5575.

[12] A. Ziabicki, P. Sajkiewicz, Crystallization of polymers in variable external conditions. III: Experimental determination of kinetic characteristics, Colloid. Polym. Sci. 276 (1998) 680-689.

[13] A. Toda, Periodically modulated driving force applied to polymer crystallization in a visco-elastic measurement with temperature modulation, Thermochim. Acta 391 (2002) 81-86.

[14] M. Zinet, R. El Otmani, M'h. Boutaous, P. Chantrenne, Numerical Modeling of Nonisothermal Polymer Crystallization Kinetics: Flow and Thermal Effects. Polym. Eng. Sci. 50 (2010) 2044-2059.

[15] A. Durin, J.-L. Chenot, J.-M. Haudin, N. Boyard, J.-L. Bailleul, Simulating polymer crystallization in thin films: Numerical and analytical methods, Eur. Polym. J. 73 (2015) 1-16.

[16] J. Guo, K.A. Nahr, Simplified model of stress-induced crystallization kinetics of polymers, Adv. Polym. Tech. 21 (2002) 214-222.

[17] L. Jarecki, B. Misztal-Faraj, Kinetic model of polymer crystallization with the lamellar thickness distribution, Eur. Polym. J. 73 (2015) 175-190.

[18] Z.J. Liu, J. Ouyang, W. Zhou, X.D. Wang, Numerical simulation of the polymer crystallization during cooling stage by using level set method, Comput. Mater. Sci. 97 (2015) 245-253.

[19] D. Raabe, A Godara, Mesoscale simulation of the kinetics and topology of spherulite growth during crystallization of isotactic polypropylene (iPP) by using a cellular automaton, Modelling Simul. Mater. Sci. Eng. 13 (2005) 733-751.

[20] R. Spina, M. Spekowius, K. Küsters, C. Hopmann, Multiphysics simulation of thermoplastic polymer crystallization, Mater. Des. 95 (2016) 455-469.

[21] R. Spina, M. Spekowius, R. Dahlmann, C. Hopmann, Analysis of polymer crystallization and residual stresses in injection molded parts. Int. J. Precis. Eng. Manuf. 15 (2014) 89-96.

[22] E. Weiman, Principles of multiscale modeling, Cambridge University Press, New York, 2011.

[23] D.F. Heaney, R. Spina, Numerical analysis of debinding and sintering of MIM parts, J. Mater. Process. Technol. 191 (2007) 385-389.

[24] J.E.K. Schawe, P.A. Vermeulen, M. van Drongelen, Two processes of -phase formation in polypropylene at high supercooling, Thermochim. Acta 616 (2015) 87-91.

[25] D. Mileva, R. Androsch, E. Zhuravlev, C. Schick, B. Wunderlich, Isotropization, perfection and reorganization of the mesophase of isotactic polypropylene, Thermochim. Acta 522 (2011) 100-109.

[26] M. Doi, S.F. Edwards. The Theory of Polymer Dynamics, University Press, Oxford, 1988.

[27] M. Spekowius, R. Spina, C. Hopmann, Mesoscale simulation of the solidification process in injection moulded parts, J. Polym. Eng. 36 (2016) 563-573.

[28] G. Lamberti, A direct way to determine iPP density nucleation from DSC isothermal measurements, Polym. Bull. 52 (2004) 443-449.

[29] Y.P. Khanna, Rheological mechanism and overview of nucleated crystallization kinetics, Macromolecules 26 (1993) 3639-3643.

[30] E. Eckestein et al., Determination of plateau moduli and entanglement molecular weights of isotactic, syndiotactic, and atactic polypropylenes synthesized with metallocene catalysts, Macromolecules 31 (1998) 1335-1340.

[31] G. Lamberti, Isotactic polypropylene crystallization: Analysis and modeling, Eur. Polym. J. 47 (2011) 1097-1112.

[32] H. Janeschitz-Kriegl, How to understand nucleation in crystallizing polymer melts under real processing conditions, Colloid. Polym. Sci. 281 (2003) 1157-1171.

[33] F. De Santis, G. Lamberti, G.W.M. Peters, V. Brucato, Improved experimental characterization of crystallization kinetics, Eur. Polym. J. 41 (2005) 2297-2302.

[34] S. Qiu, Y. Zheng, A. Zeng, Y. Guo, Prediction of non-isothermal crystallization parameters for isotactic polypropylene, Thermochim. Acta 512 (2011) 28-33.

[35] S. Coppola, L. Balzano, E. Gioffredi, P.L. Maffettone, N. Grizzuti, Effects of the degree of undercooling on flow induced crystallization in polymer melts, Polymer 45 (2004) 3249-3256.

[36] A. Gooneie, S. Schuschnigg, C. Holzer, Coupled orientation and stretching of chains in mesoscale models of polydisperse linear polymers in startup of steady shear flow simulations, Macromol. Theory Simul. 25 (2016) 170-186.

Table(s)

	Parameter	Value		Description
	$t_{½,0}$	1.74×10^{14}	1/s	Half time in equilibrium condition
	U^*	1.72×10^{4}	J/mole	Activation energy for the segmental jump rate
MACRO	$T_{m,0}$	467.15	K	Equilibrium melt temperature
MACRO	T_g	263.15	K	Glass transition temperature
MACRO	T_∞	51.60	K	Temperature below which the diffusion stops
	$\varkappa_t$	3.1710	-	Parameter associated to spherulite growth rate
	n	4	-	Avrami exponent
	C	2.50×10^{40}	$1/(J^2\times s)$	Nucleation amplitude
	K_{nuc}	3.42×10^{18}	$(J\times s)/m^3$	Crystallization constant of nucleation
MESO	E_a	7.68×10^{3}	J	Energy barrier of the nucleation
MESO	$\varkappa_g$	2.7979	-	Crystallization growth constant
	$v_{g,0}$	4.36×10^{8}	m/s	Equilibrium growth amplitude
	n	2	-	Geometrical factor for the nucleation model

Table 1: Parameters of the material model

Figure(s)

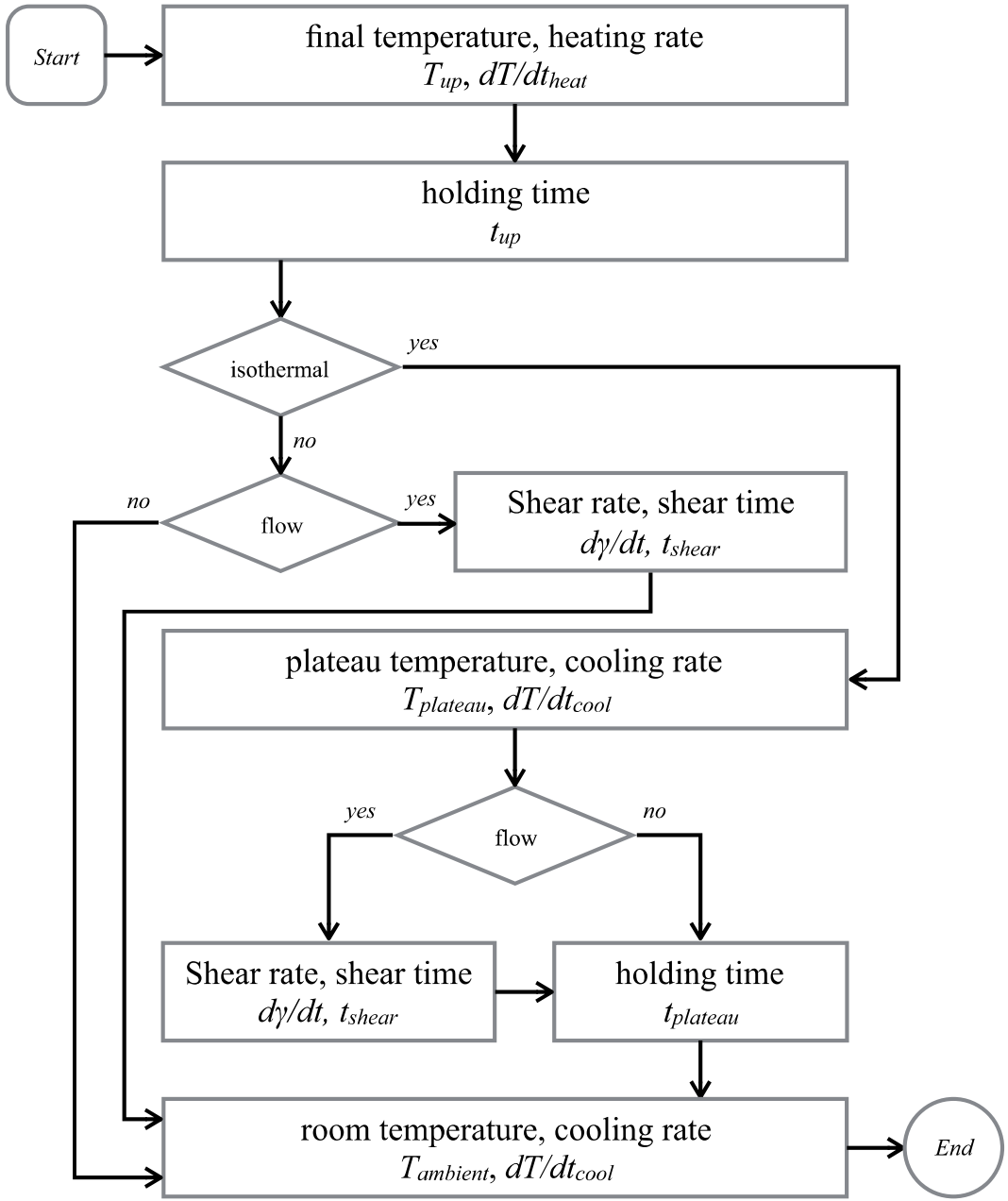

Figure 1: Experiment flow diagram

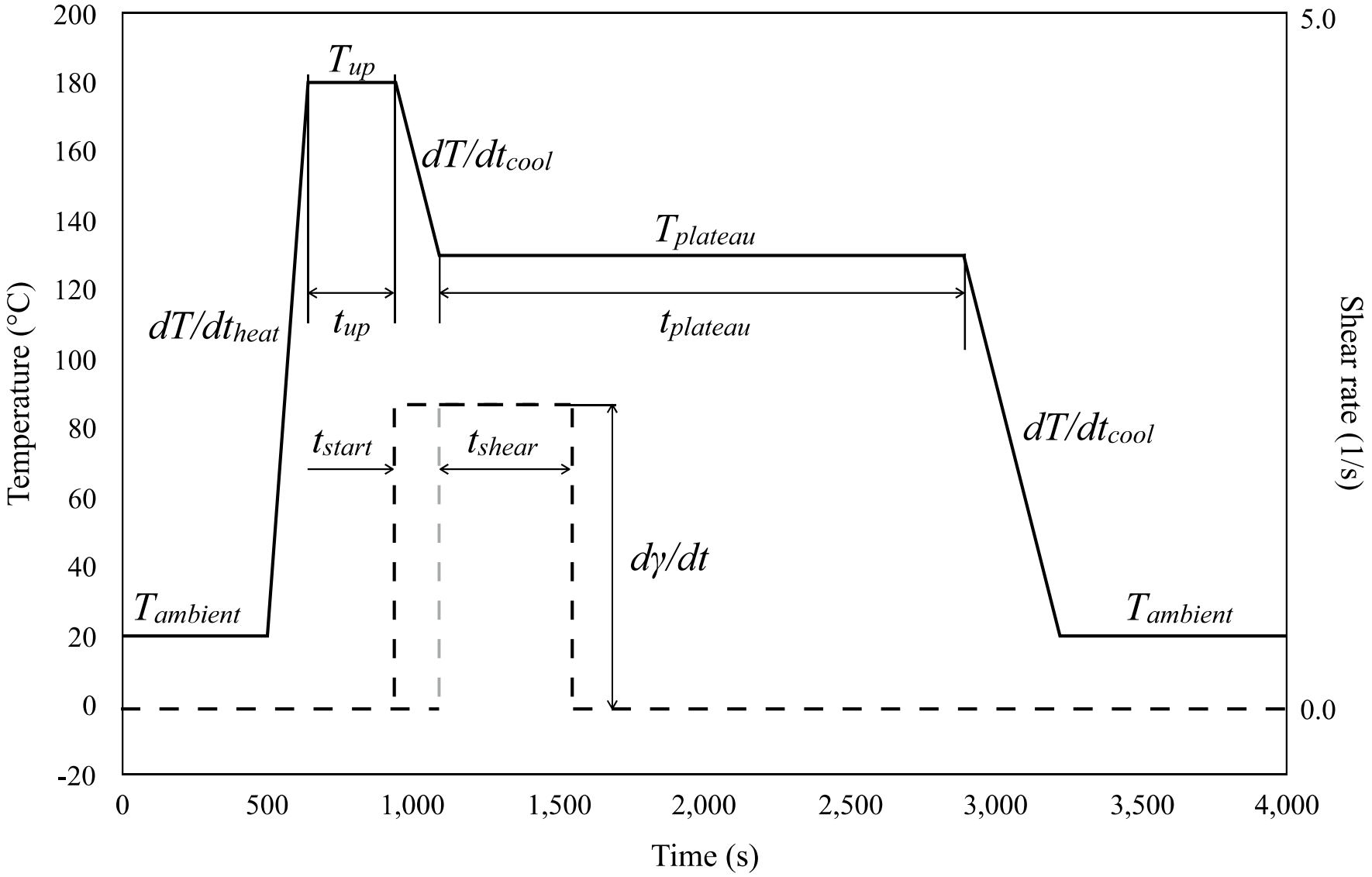

Figure 2: Thermal Cycle

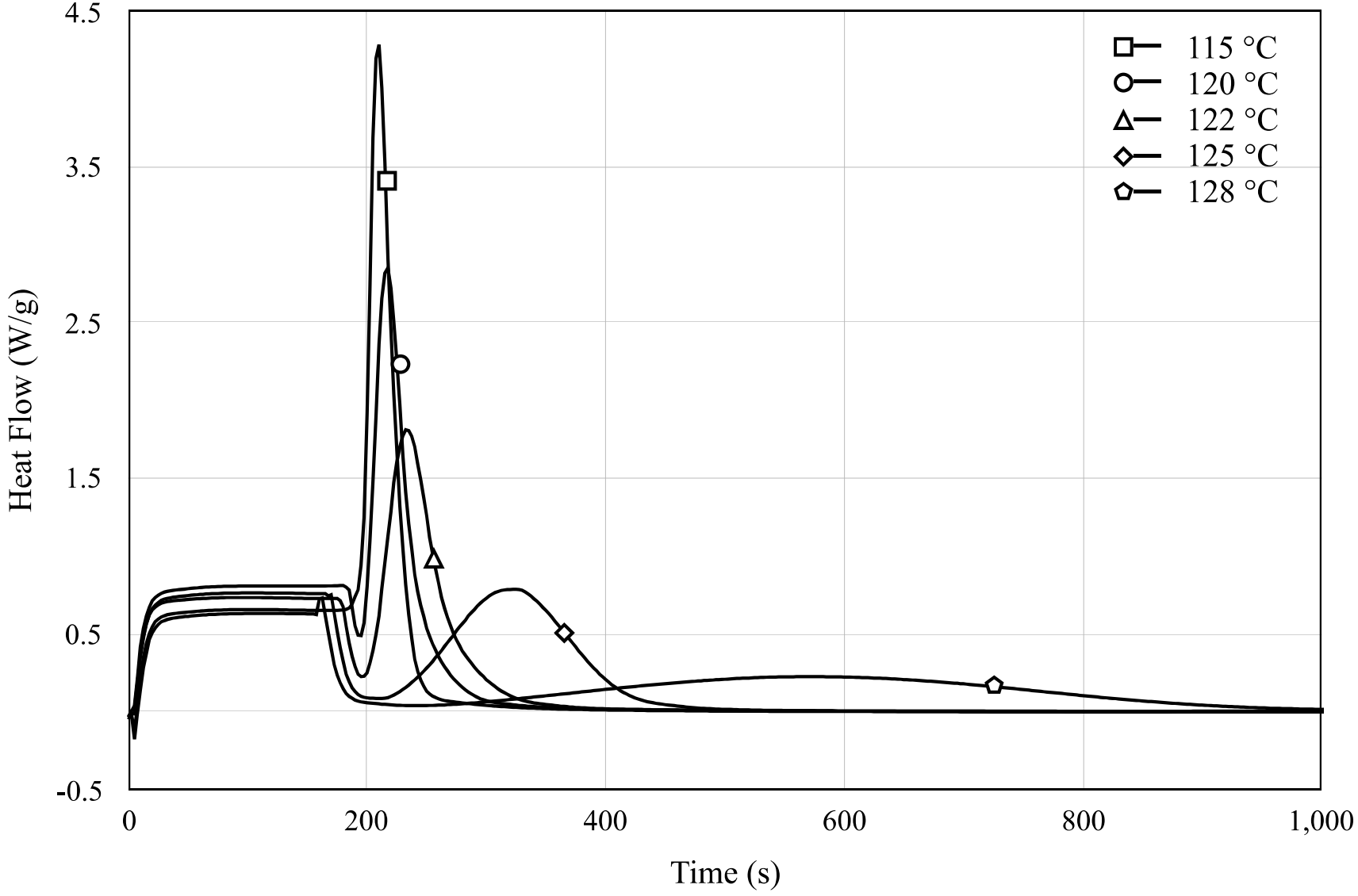

Figure 3: Isothermal DSC curves

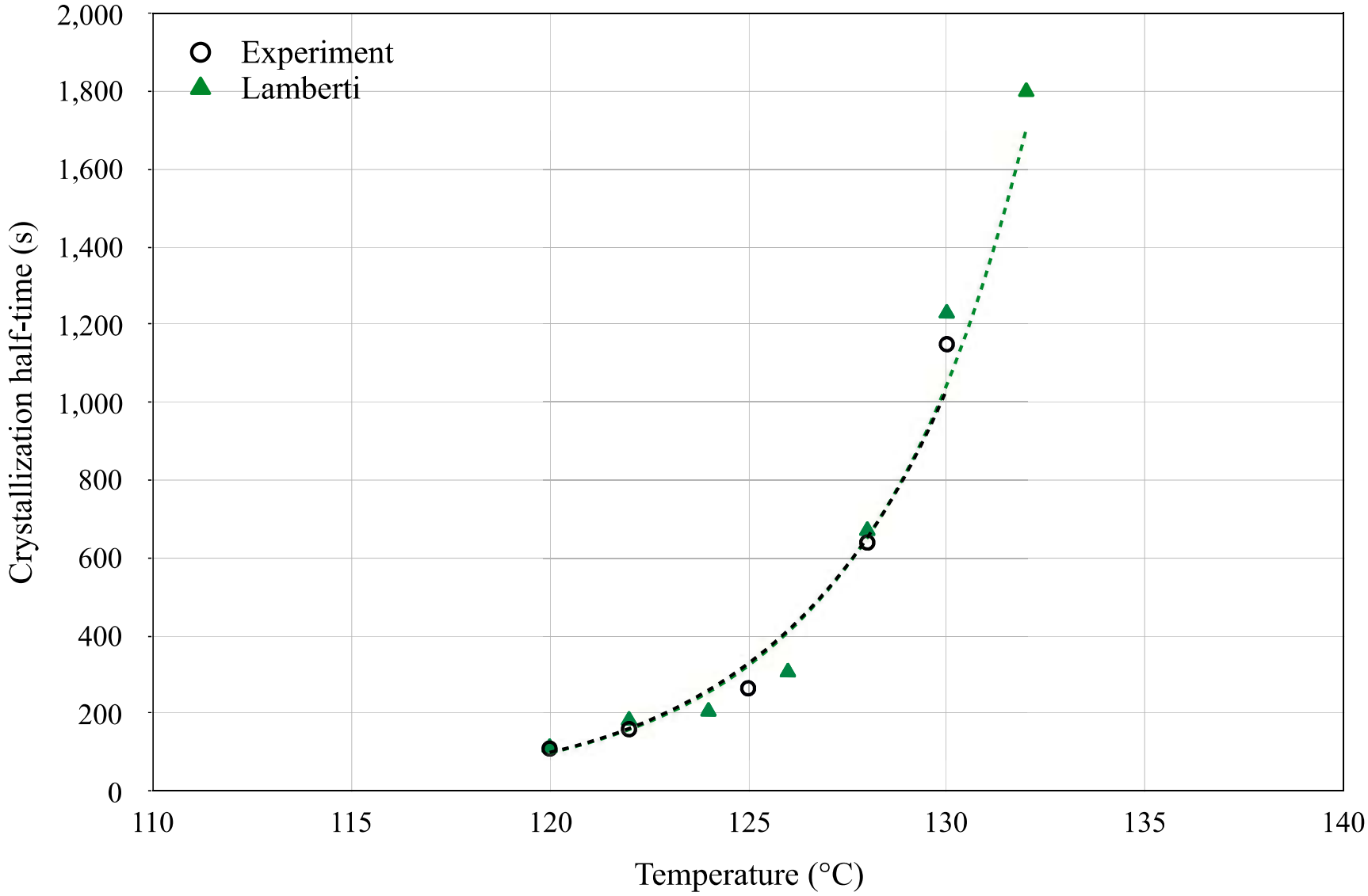

Figure 4: Isothermal half-time

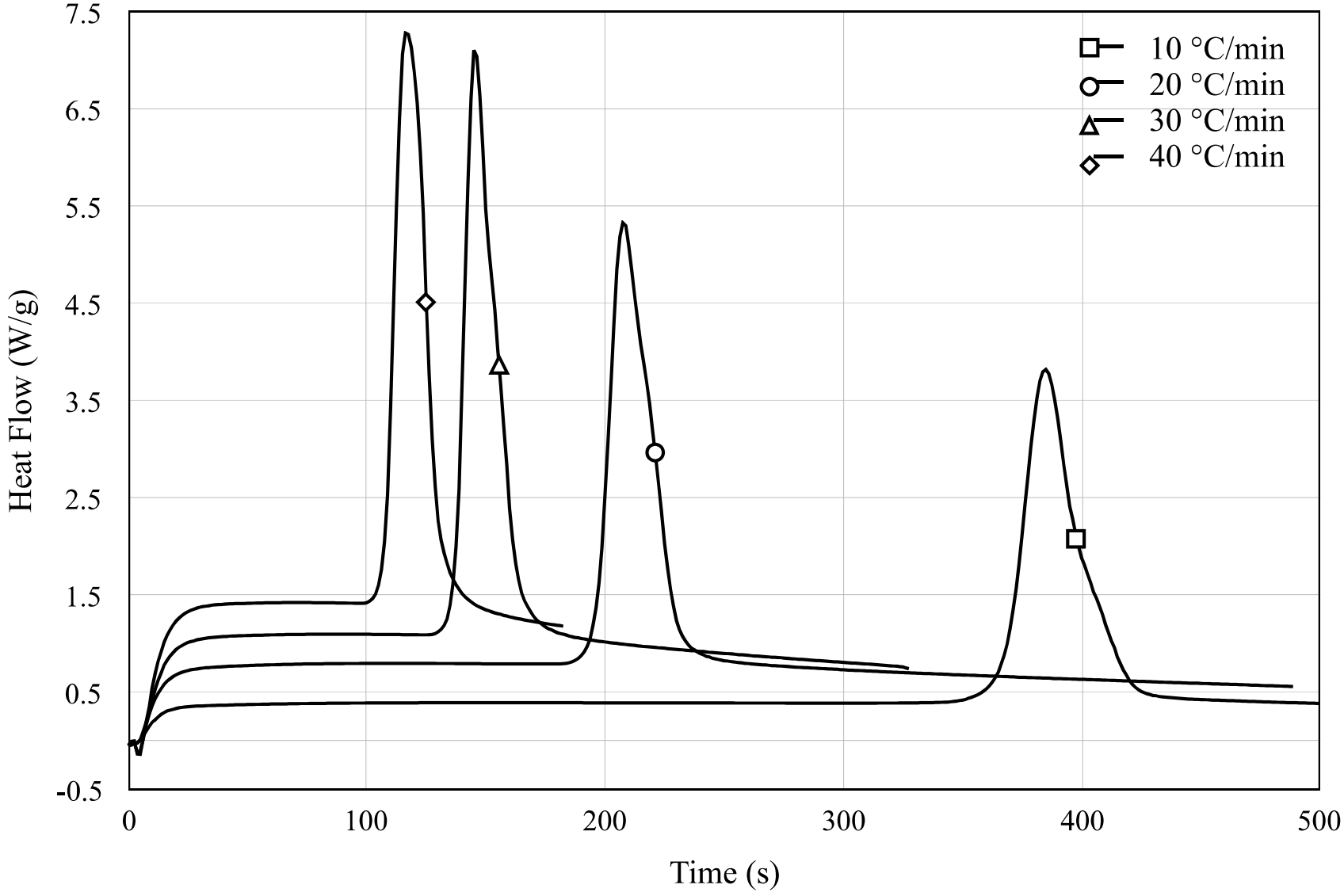

Figure 5: Non-isothermal DSC curves

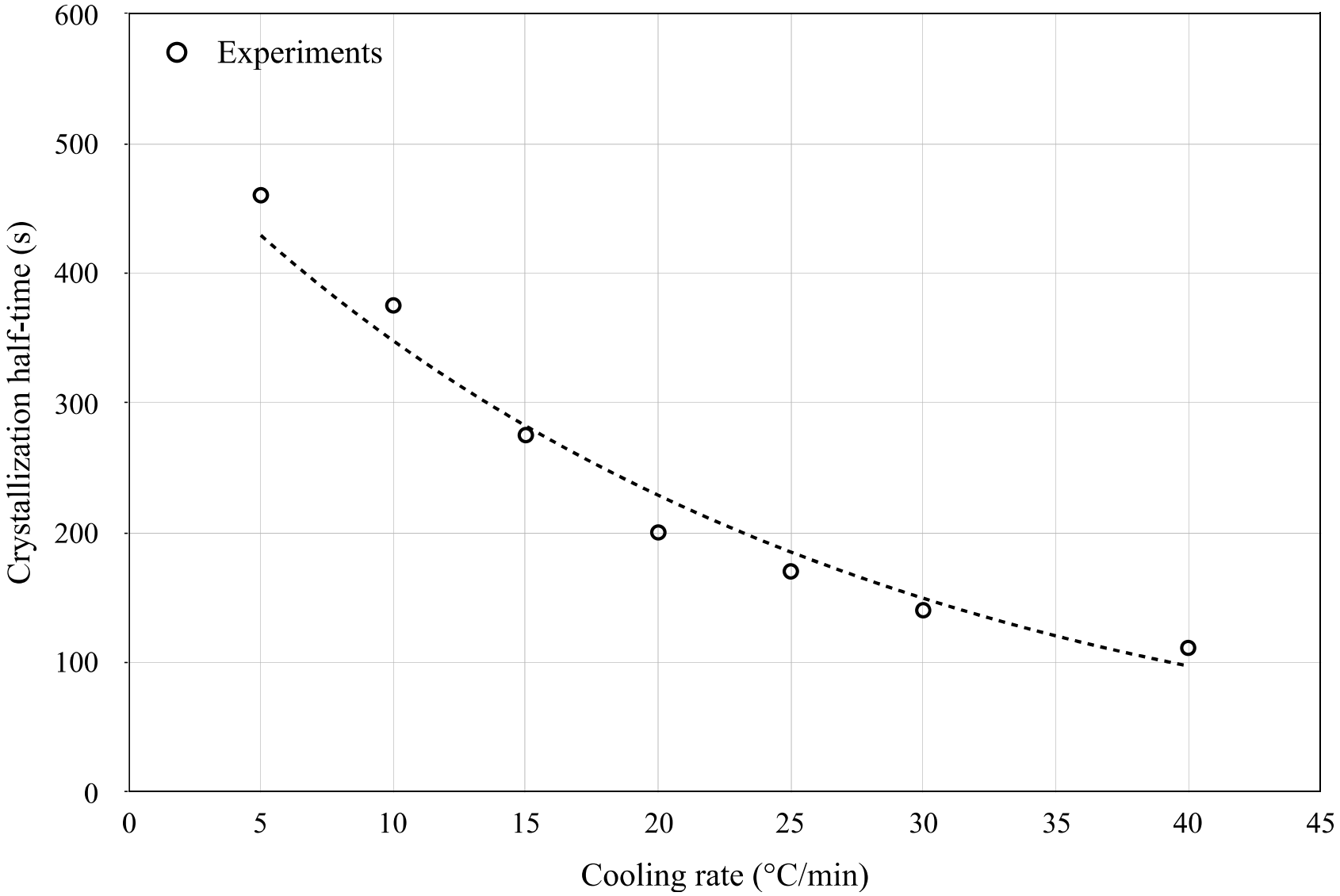

Figure 6: Non-isothermal half-time

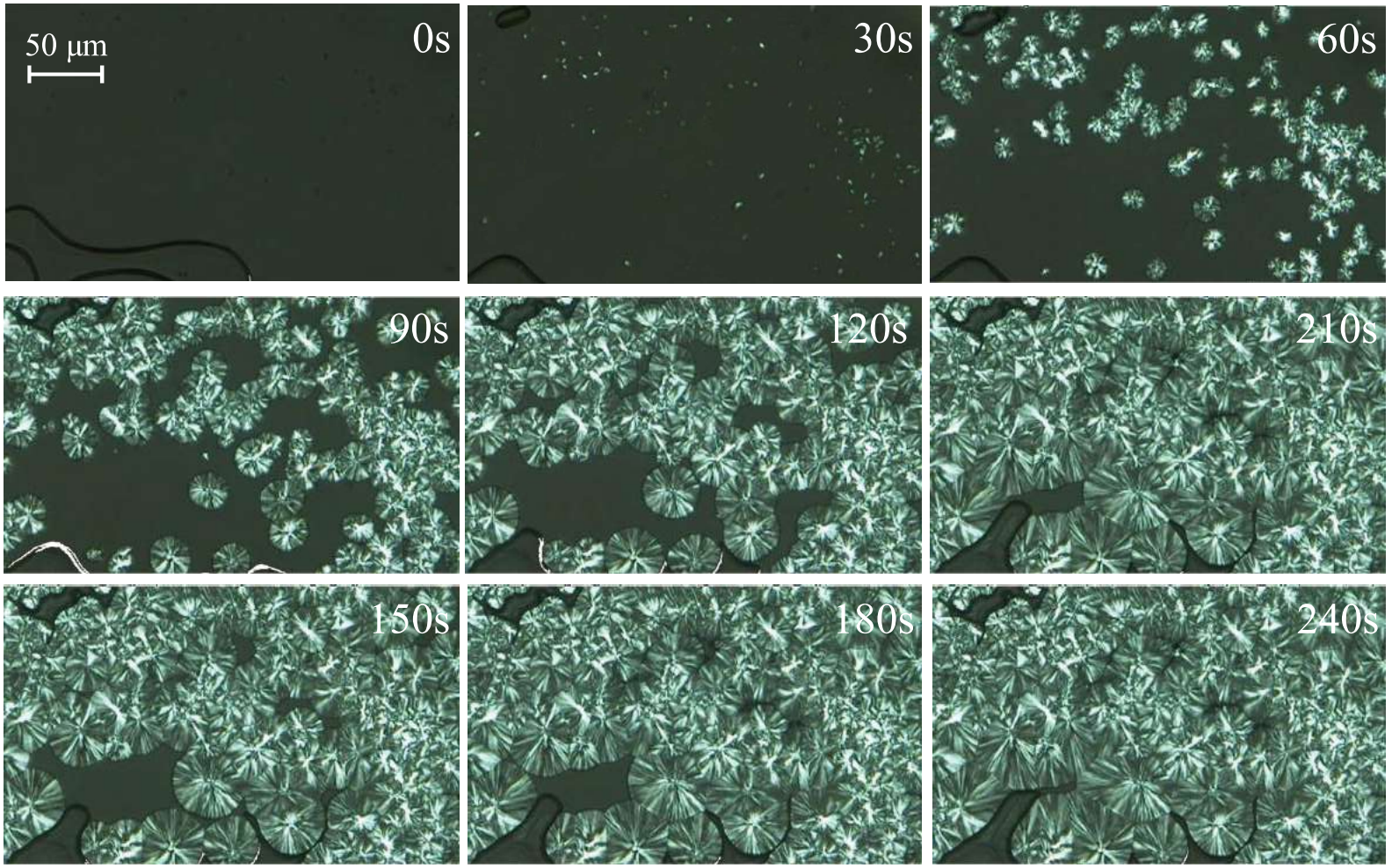

Figure 7: Polymer melt during cooling

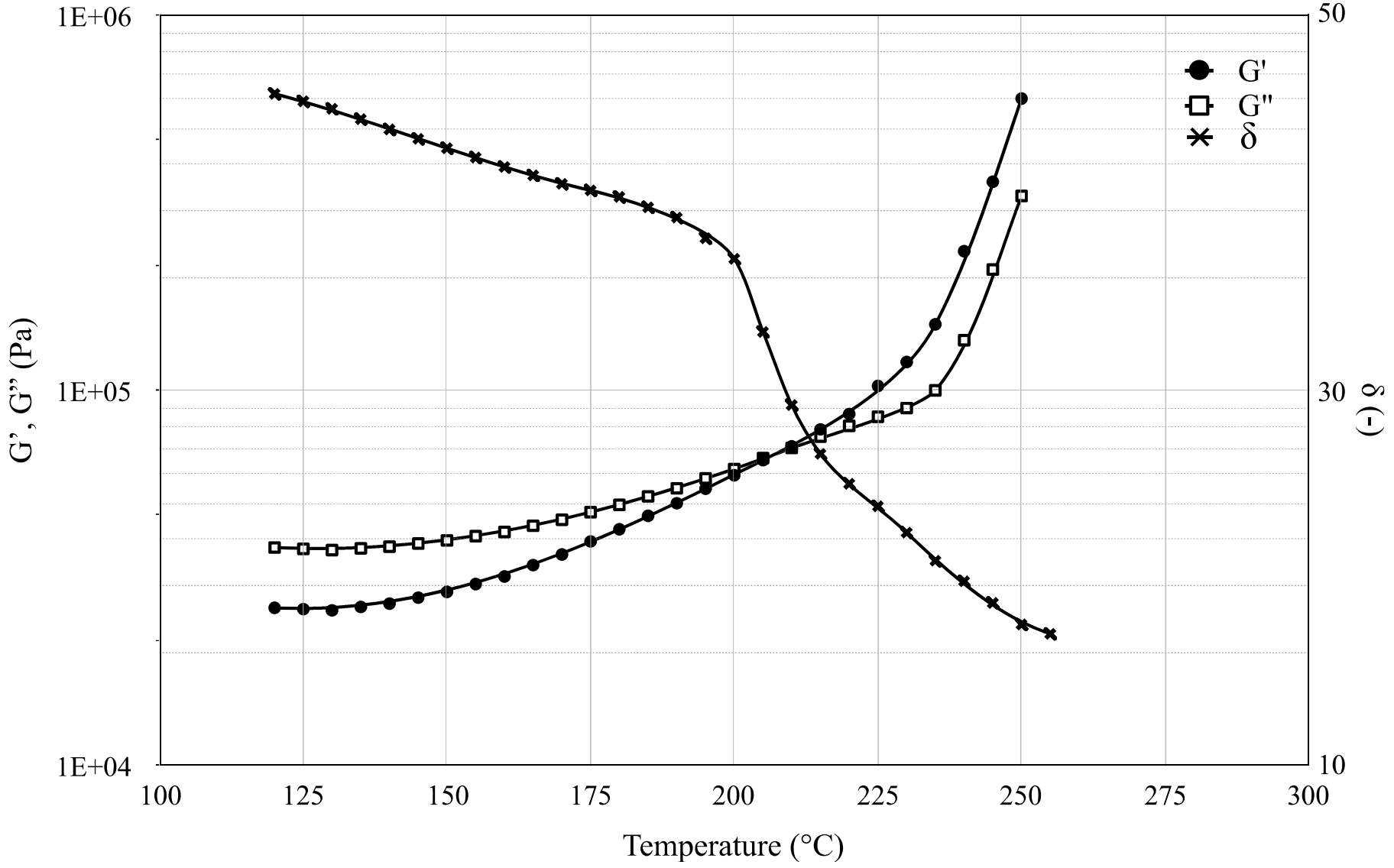

Figure 8: Rheometer curves

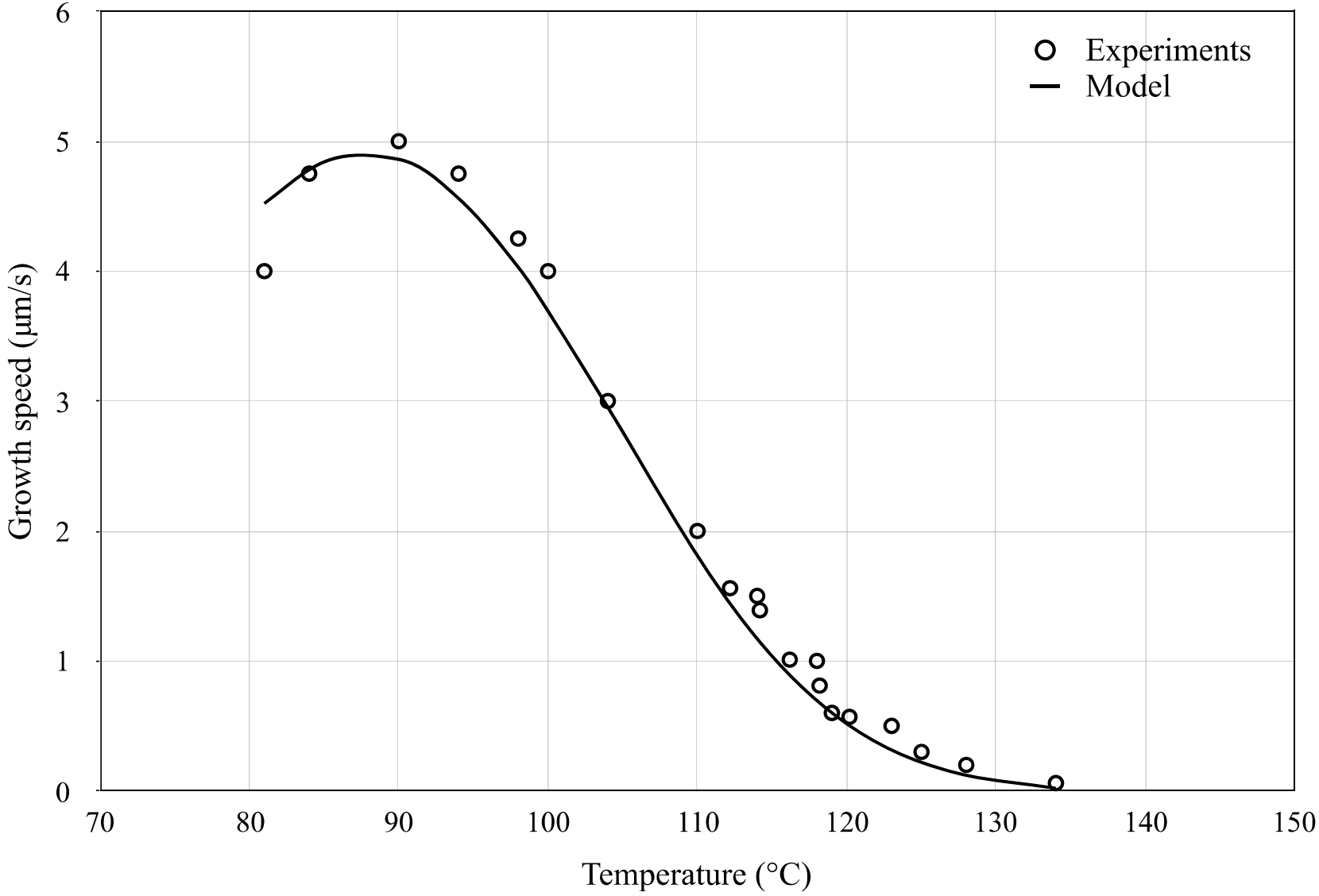

Figure 9: Growth speed

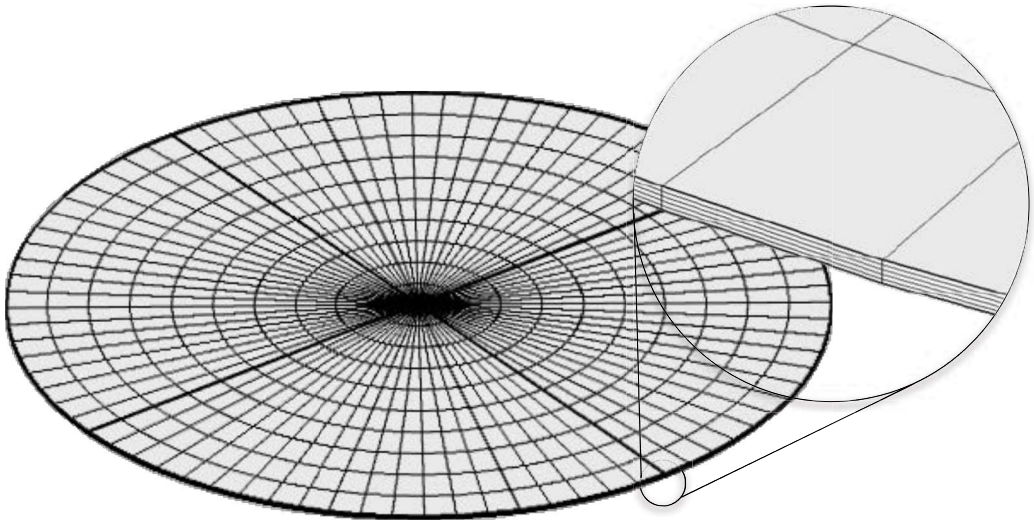

Figure 10: FE model

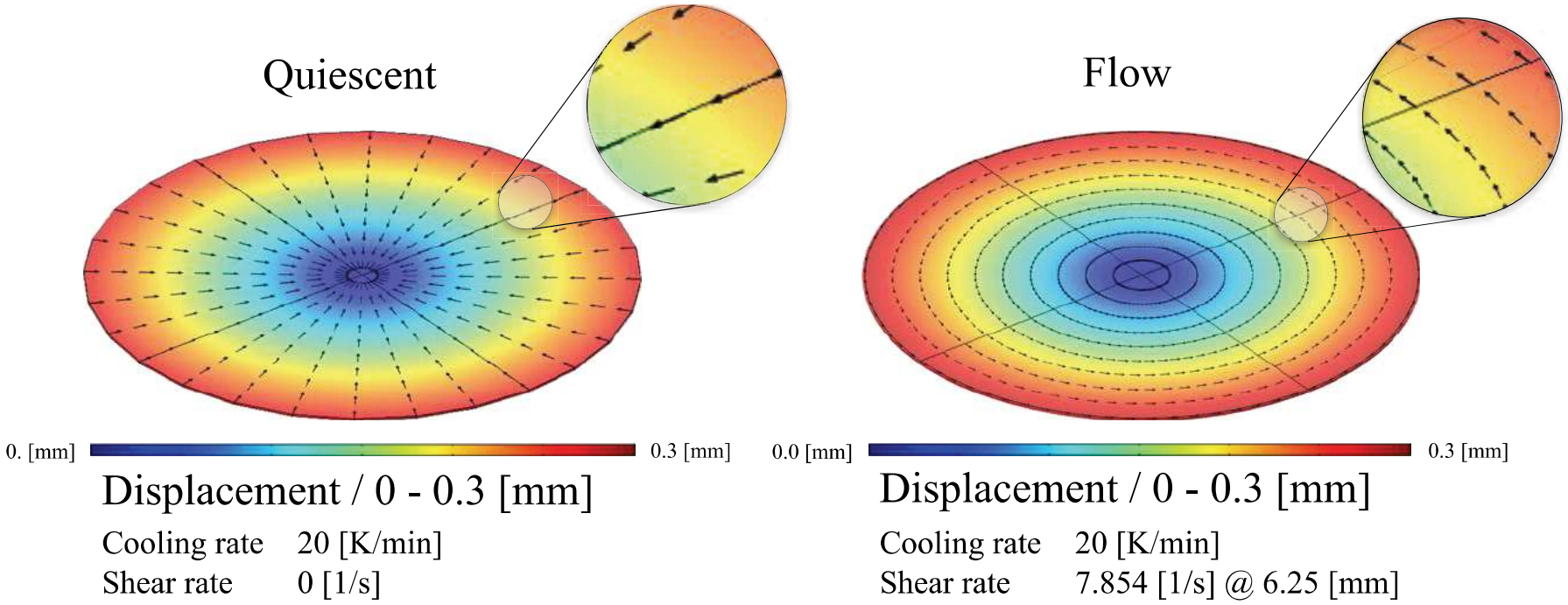

Figure 11: Displacement

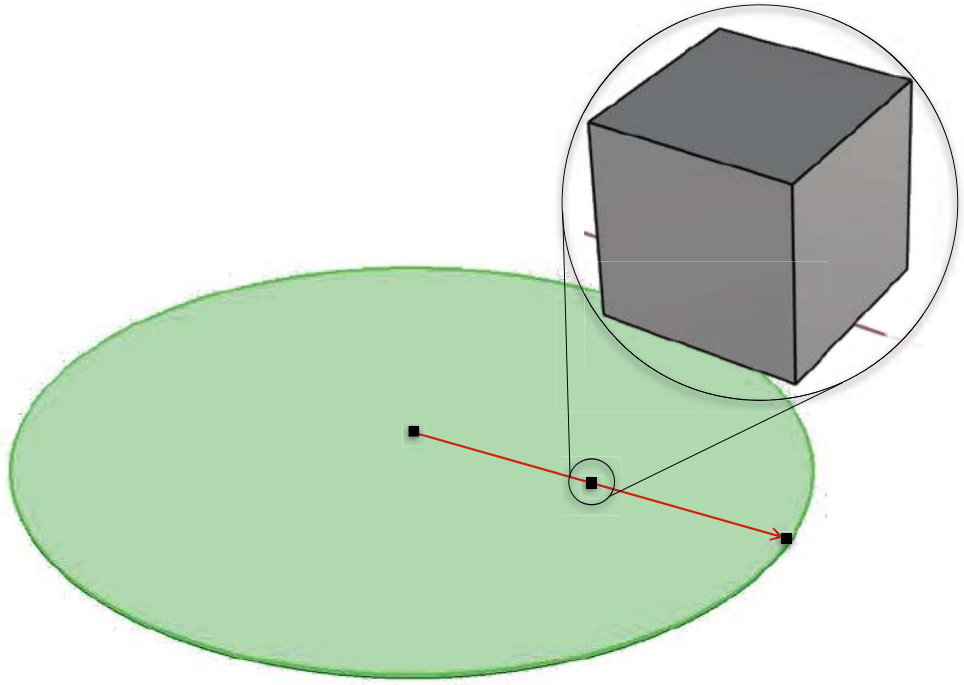

Figure 12: Volumes of analysis

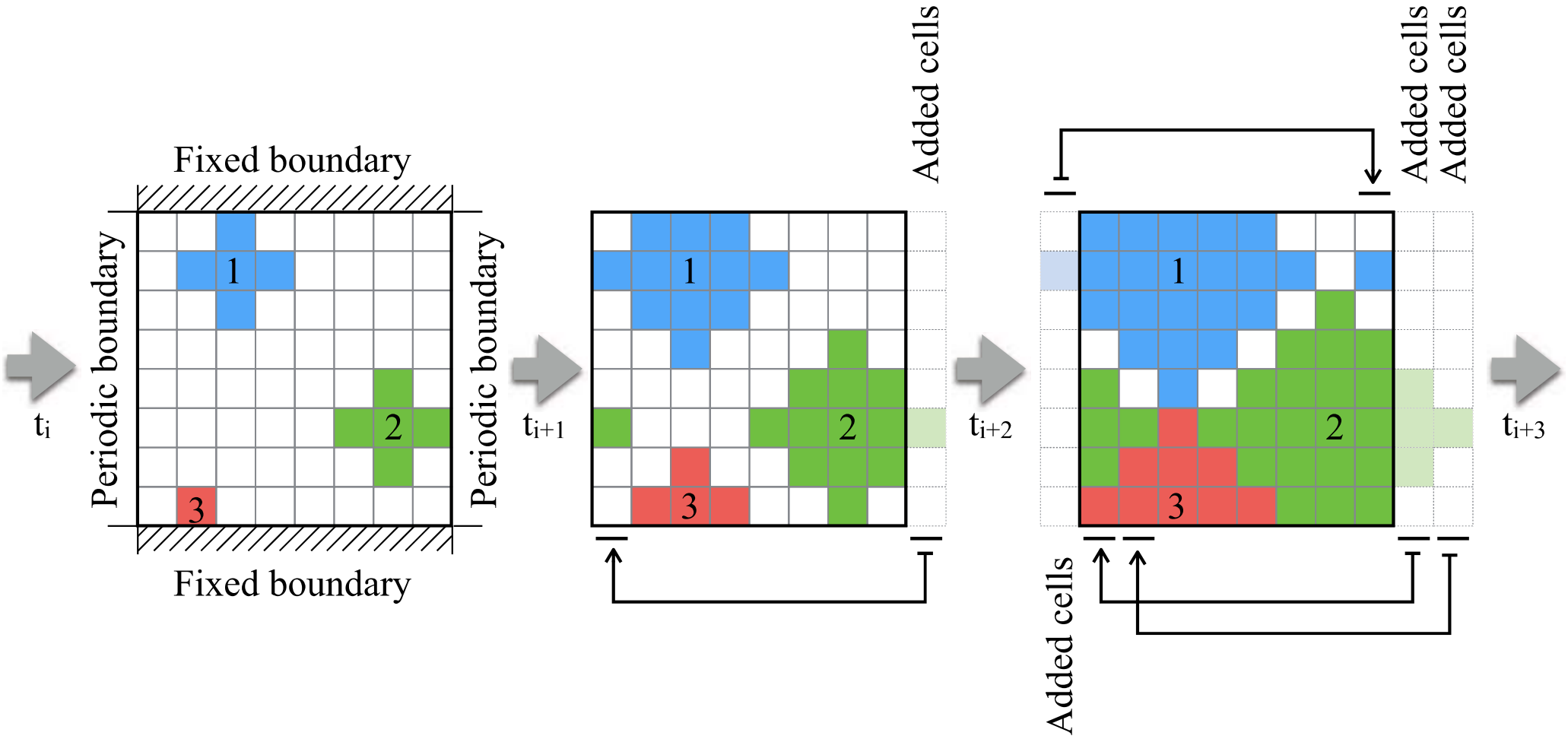

Figure 13: Spherulite growth

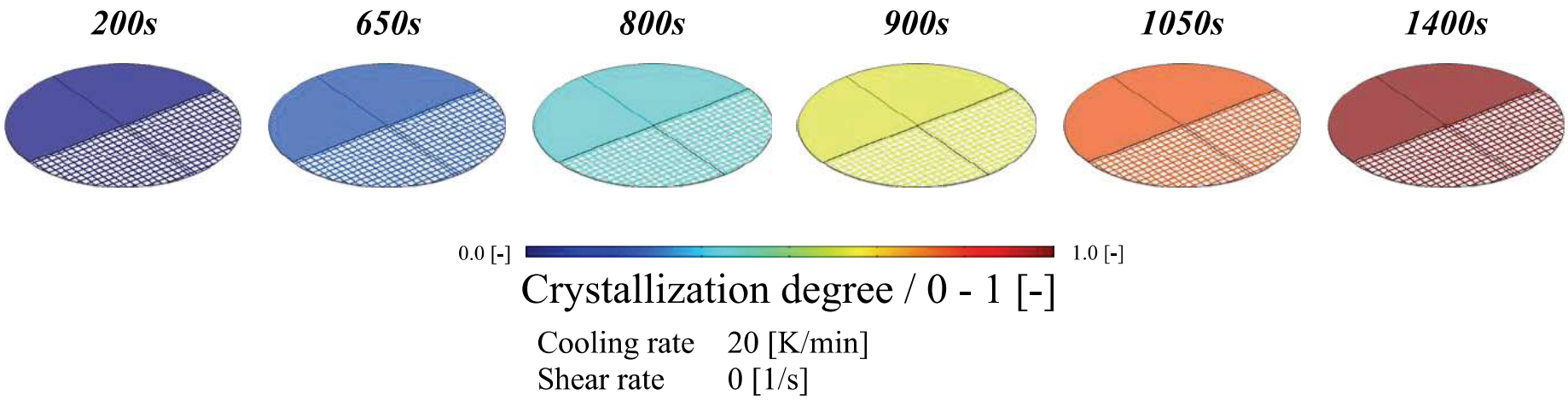

Figure 14: Crystallization degree at 130°C \ FE model

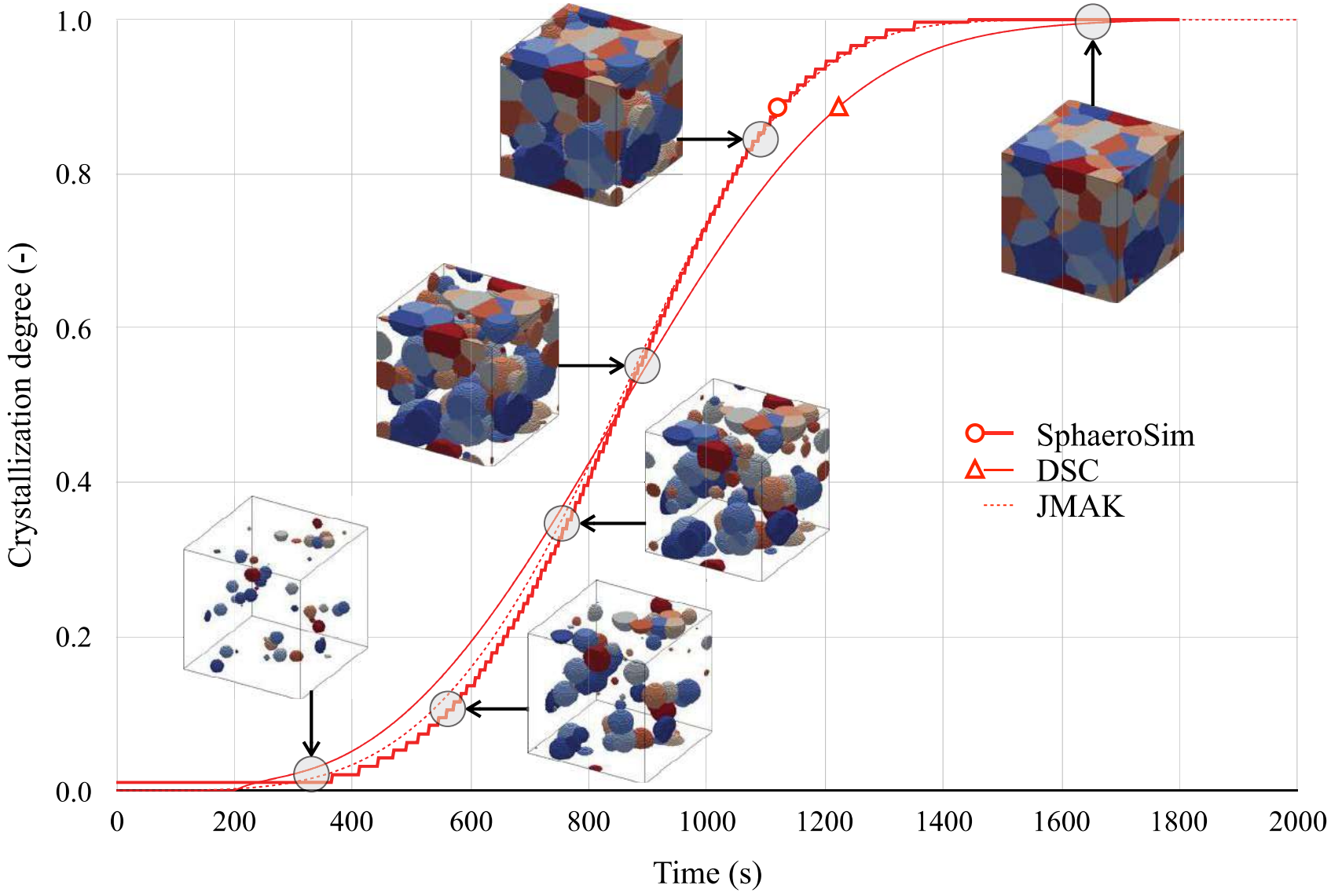

Figure 15: Crystallization degree at 130°C

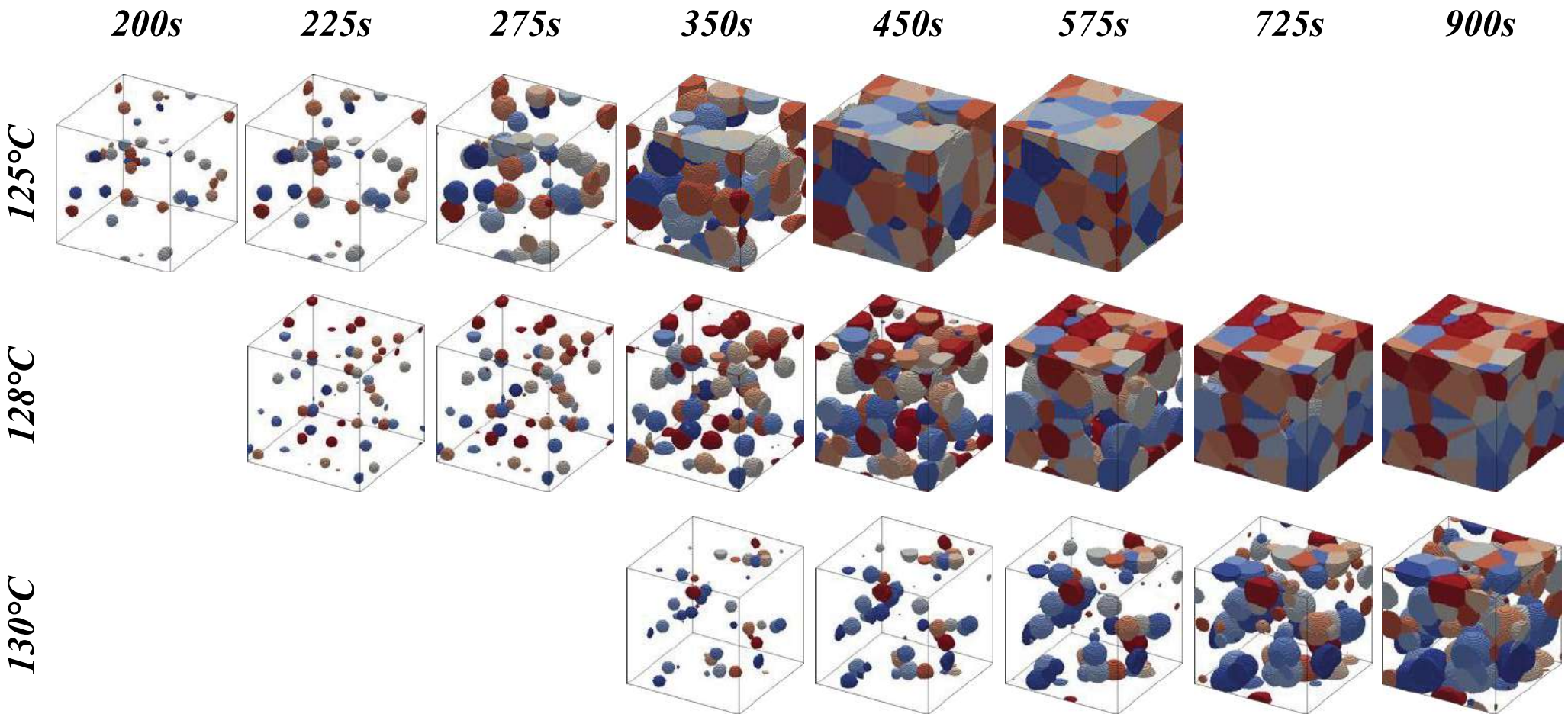

Figure 16: Spherulite evolution \ Isothermal

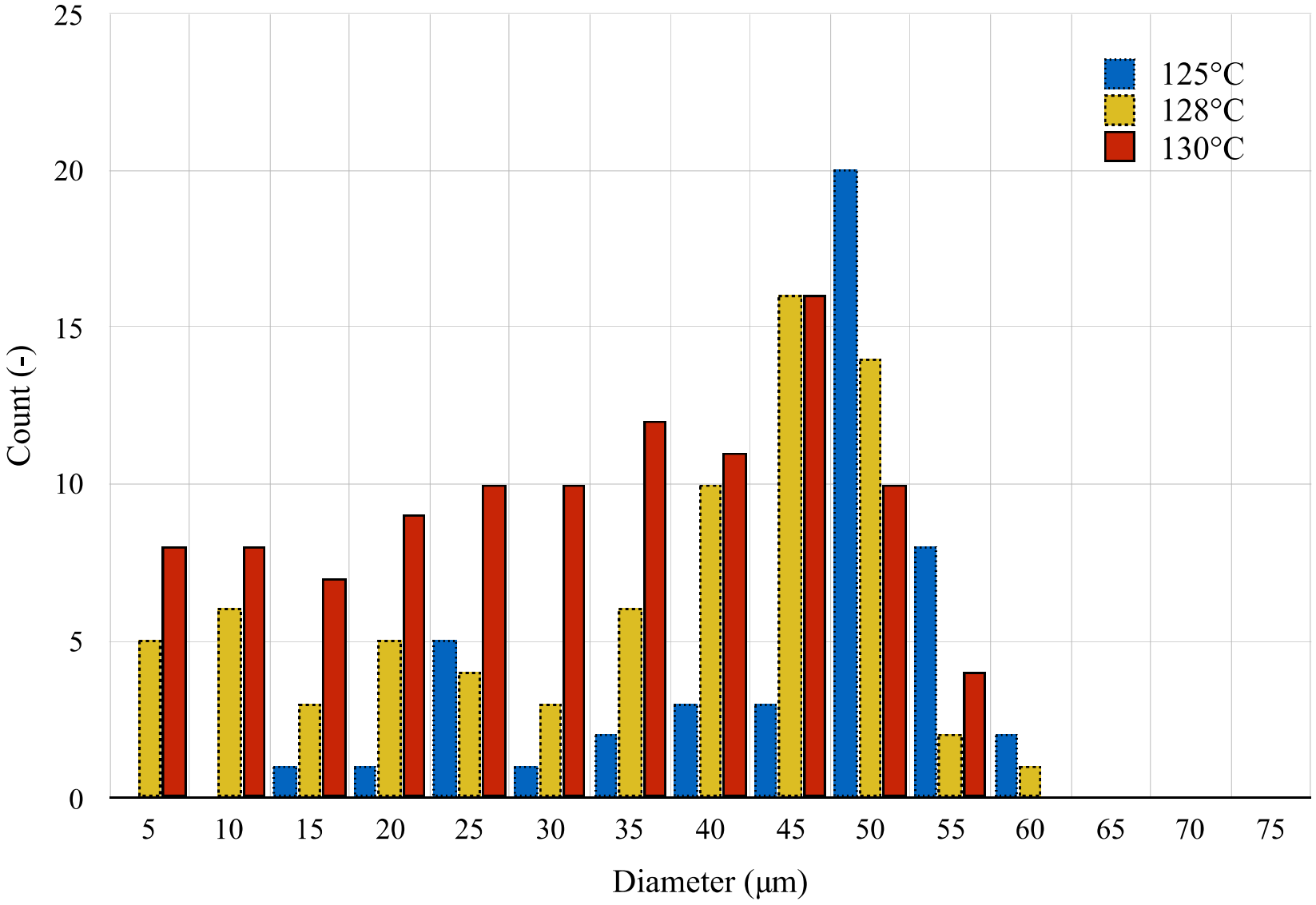

Figure 17: Spherulite distribution \ Isothermal

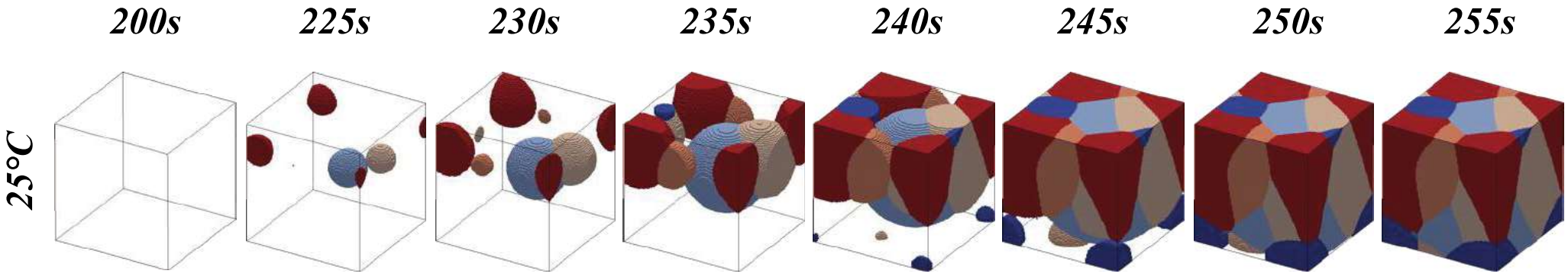

Figure 18: Spherulite evolution at 25°C \ Non-isothermal

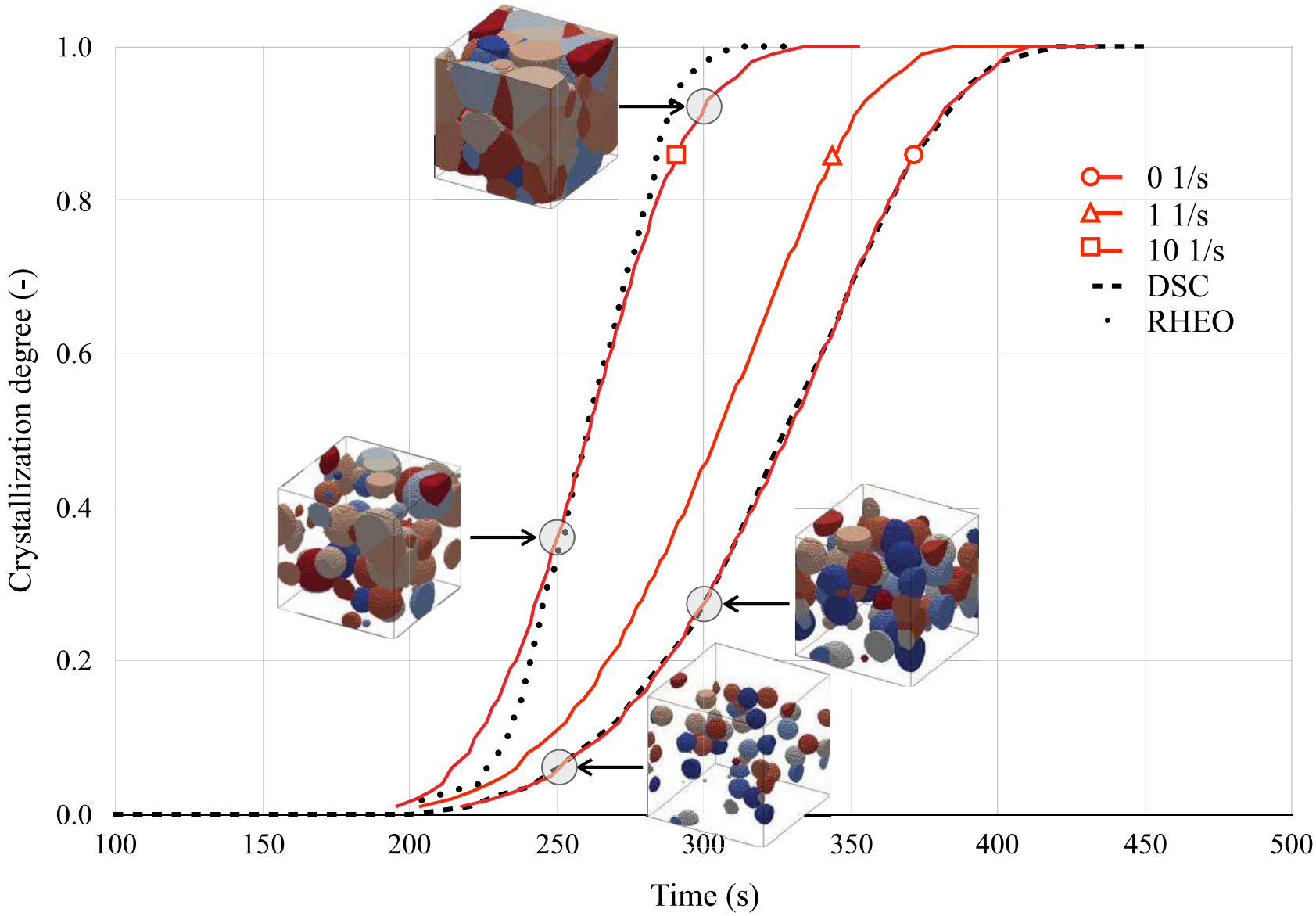

Figure 19: Crystallization degree at 125°C

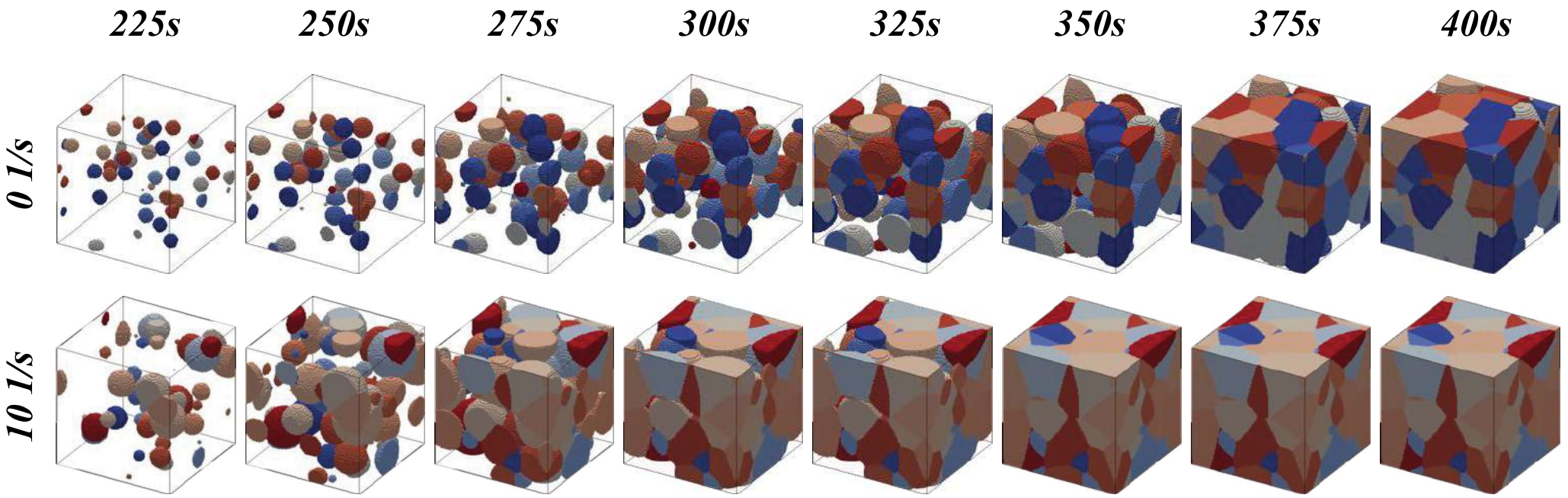

Figure 20: Spherulite evolution at 125°C \ Shear influence

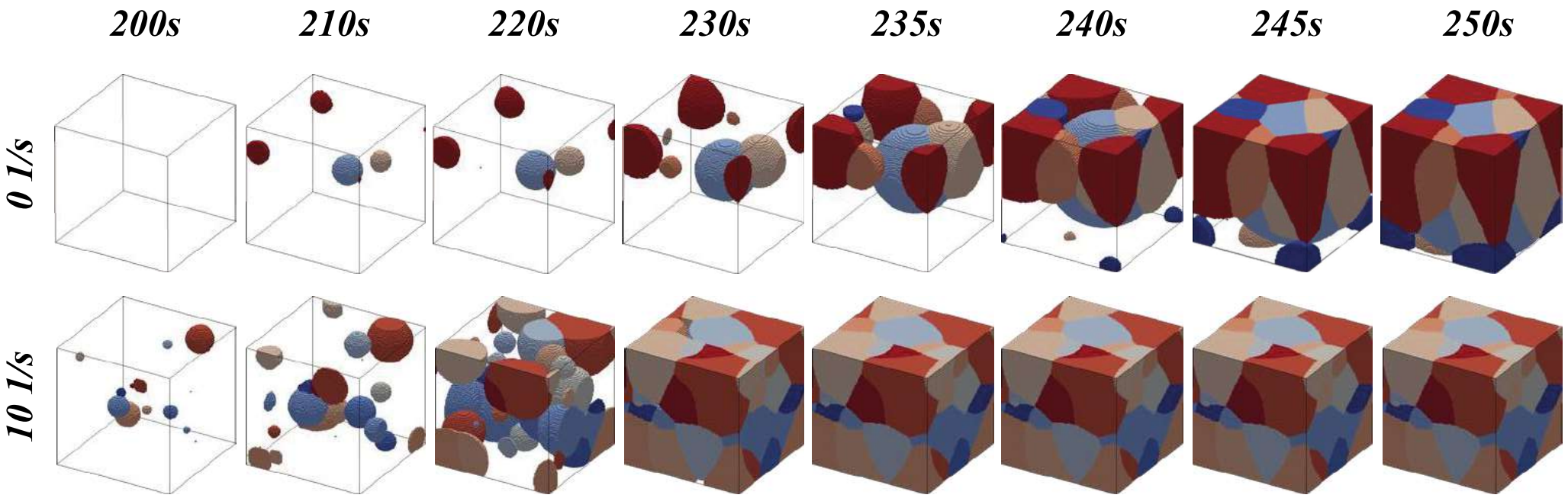

Figure 21: Spherulite evolution at 25°C \ Shear influence